Contrib Mineral Petrol (2001) 141: 572–591
DOI 10.1007/s004100100261

B. Bühn · F. Wall · M.J. Le Bas

Rare-earth element systematics of carbonatitic fluorapatites, and their significance for carbonatite magma evolution

Received: 28 November 2000 / Accepted: 19 February 2001 / Published online: 8 May 2001

Abstract Magmatic fluorapatites of five African carbonatite complexes were analyzed for rare-earth (REE) and trace elements by electron microprobe and high-resolution synchrotron micro-XRF to explore the fluorapatite composition during different stages of carbonatite magma evolution. Early crystallized fluorapatites have La concentrations mostly below 1,500 ppm and low ΣREE. They display convex-upward shaped REE patterns with $(La/Nd)_{cn} \leq 1$ and low $(La/Yb)_{cn}$ ratios < 100. In contrast, fluorapatites from fractionated carbonatites have straight REE patterns with $(La/Nd)_{cn} > 1$ and $(La/Yb)_{cn}$ generally above 100, and have La up to 1 wt% at a high ΣREE. Model calculations with the fractionating mineral assemblage fluorapatite + calcite ± clinopyroxene suggest REE distribution coefficients for fluorapatite/carbonatite melt with a positive slope throughout from La to Lu, in order to meet the relationships observed in the natural fluorapatites. The calculations oppose closed system conditions of magma fractionation along the liquid lines of descent, but suggest periods of instantaneous fluorapatite crystallization. Fluorapatite trace element characteristics are therefore thought to be indicative for carbonatite evolution, and can reflect the relative degree of magma fractionation. We suggest that the $(Eu/Eu^*)_{cn}$ and Y evolution in the fluorapatites is a manifestation of an aqueous fluid immiscibly coexisting with the carbonatite magma from early evolution on, which is able to continuously extract divalent Eu and Y from the carbonatite magma.

B. Bühn (✉)
Institut für Geowissenschaften und Lithosphärenforschung,
Universität Giessen, Senckenbergstrasse 3,
35390 Giessen, Germany
E-mail: Bernhard.Buehn@geolo.uni-giessen.de
Tel.: +49-641-9936057
Fax: +49-641-9936059

F. Wall
Department of Mineralogy, The Natural History Museum,
Cromwell Road, London SW7 5BD, UK

M.J. Le Bas
School of Ocean and Earth Science, Southampton University,
European Way, Southampton SO14 3HZ, UK

Editorial responsibility: J. Hoefs

Introduction

Fluorapatite is a frequent liquidus phase in carbonatite magmas (Eby 1975; Le Bas and Handley 1979; Eriksson et al. 1985; Le Bas 1989; Walter et al. 1995), and is also known to crystallize throughout carbonatite fractionation (Hogarth et al. 1985; Hogarth 1989; Gittins 1989). At high modal abundance, fluorapatite may form igneous phoscorites (Kapustin 1980, and references therein; Eriksson 1989; Mariano 1989) or occur as layered and lensoid bodies in many carbonatite complexes. In principle, its abundance and common occurrence in carbonatitic rocks favors fluorapatite as a petrogenetic and geochemical indicator mineral (e.g., Le Bas et al. 1992; Stoppa and Liu 1995) which, however, requires knowledge of trace element distribution coefficients for the fluorapatite/carbonatite melt system which are currently unknown. Qualitative indications only can be derived for the rare-earth elements (REE) from experimental studies on apatite/fluid (Ayers and Watson 1993) and apatite/phosphate–fluoride melt systems (Fleet and Pan 1997). A variety of structural aspects of REE incorporation into apatite have been investigated (Hughes et al. 1991; Fleet and Pan 1995a, 1995b; Rakovan and Reeder 1996), but the relationships between fluorapatite composition and carbonatite melt composition, distribution coefficients, or degree of fractionation have not been established for natural systems.

There are both analytical and systematic difficulties in deriving petrogenetic implications from fluorapatite composition. Because of, in places, intimate intergrowths of fluorapatite with other minerals, most compositional data published on carbonatitic fluorapatites derive from spot analysis using conventional electron

microprobe techniques yielding reliable data for the LREE only, and sometimes for even atomic numbers of the MREE. Systematic intricacies include the lack of significant amounts of fluorapatite in late-stage carbonatites because of prominent early fluorapatite fractionation (Le Bas 1999). The low viscosity and moderate density of carbonate magmas (Wolff 1994; Minarik and Watson 1995) favors the accumulation of ubiquitous liquidus phases such as fluorapatite, calcite, and clinopyroxene as partial mineral cumulates (Biggar 1969; Treiman and Schedl 1983). Accordingly, many sövites even may be considered as cumulate rocks (Wyllie 1989; le Roex and Lanyon 1998; Bühn et al. 2001). A direct comparison between fluorapatite and host rock composition taken as parental melt is therefore hampered. These limitations mean that only a few studies have been able to consider fluorapatite chemistry as a function of carbonatite differentiation in order to use fluorapatite composition as a tracer for magma evolution (Stoppa and Liu 1995; Walter et al. 1995). This study investigates the fluorapatite composition in calciocarbonatites (sövites) and cumulates which represent different degrees of differentiation. It explores whether fluorapatite composition monitors the evolution of carbonatite magmas, with the aim of assessing the systematics of trace element incorporation into fluorapatite in natural carbonatite magmas.

Previous work and rationale

Rare-earth element patterns of magmatic, carbonatitic fluorapatites from previous studies are shown in Fig. 1, excluding carbonatitic fluorapatites that are thought to be affected by hydrothermal alteration. Except for the beforsite host rock of the Juquiá carbonatite (Walter et al. 1995), all other host rocks to the fluorapatites are sövites. The data indicate that the diversity of carbonatitic, magmatic fluorapatite REE patterns is far more pronounced than may be suggested by the "average carbonatitic apatite" derived from 111 carbonatitic apatite analyses by Fleischer and Altschuler (1986). There appear to be two qualitatively different groups of fluorapatites. One group (Phalaborwa and Siilinjärvi) displays a rather flat pattern at the LREE end of the REE spectrum. The other group (e.g., Oka samples) displays a straight REE pattern throughout. All intermediate REE patterns are developed. To quantify the shape and the slope of the fluorapatite REE patterns, the chondrite-normalized ratios $(La/Nd)_{cn}$ and $(La/Yb)_{cn}$ are used here. The $(La/Nd)_{cn}$ ratios range between 1.2 and 5.0, and the ratio $(La/Yb)_{cn}$ displays a wide spread between 12 and 377. A plot of the La_{cn} content versus $(La/Yb)_{cn}$ shows a positive correlation (Fig. 1), suggesting that the slope of the REE patterns may be a function of the total concentration of La (and of ΣREE) in the fluorapatites. There are three fluorapatite REE patterns (Eby 1975; Fleischer and Altschuler 1986; Hughes et al. 1991) which have a negative $(Eu/Eu^*)_{cn}$ anomaly developed, and one

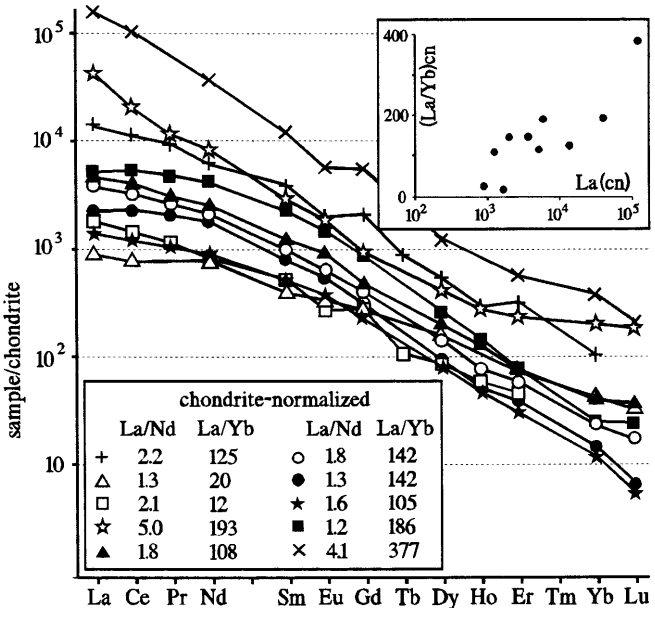

Fig. 1 Selected REE patterns of magmatic, carbonatitic apatites displaying various $(La/Nd)_{cn}$ and $(La/Yb)_{cn}$ ratios, and bulk REE contents. The *inset* shows a positive correlation between the La_{cn} content and $(La/Yb)_{cn}$. *Plus symbols* mean of 111 carbonatitic apatites (Fleischer and Altschuler 1986); *open triangles* Juquiá carbonatite, mean of five analyses (Walter et al. 1995); *open squares* Oka carbonatite, mean of eight apatite analyses (Eby 1975); *open stars* Oka carbonatite (Hornig-Kjarsgaard 1998); *full triangles* Fen carbonatite (Hornig-Kjarsgaard 1998); *open circles* Sokli carbonatite (Hornig-Kjarsgaard 1998); *full circles* Siilinjärvi carbonatite (Hornig-Kjarsgaard 1998); *full stars* Jacupiranga carbonatite (Hornig-Kjarsgaard 1998); *full squares* Phalaborwa carbonatite (Hornig-Kjarsgaard 1998); *crosses* Oka carbonatite (Hughes et al. 1991)

sample (Walter et al. 1995) may even suggest a slight negative $(Ce/Ce^*)_{cn}$ anomaly.

These data, however, do not allow a decision on whether the range of ΣREE, $(La/Nd)_{cn}$, $(La/Yb)_{cn}$, or redox-related anomalies are a function of the degree of fractionation, the initial melt composition, or both. In order to investigate these relationships, fluorapatite-bearing carbonatite samples were analyzed from different evolutionary stages of three African carbonatite complexes, and as single samples from some other African carbonatites.

Selection of natural fluorapatite samples

The samples investigated derive from six African carbonatite complexes. Except for one complex analyzed for comparison (Okorusu), all other complexes contain fluorapatite of magmatic origin without a recognizable hydrothermal overprint.

The sub-volcanic *Homa Mountain carbonatite* of western Kenya is Tertiary to Recent in age (Le Bas 1977). Samples for this study are from the Le Bas collection of The Natural History Museum, London. The fluorapatite in samples HC559 and HC554 occurs in folded, irregular layers up to 0.5 cm in thickness in a carbonate matrix. The fluorapatite layers consist of fine-grained fluorapatite with individual grain sizes on the micrometer scale. Fine-grained carbonate is interspersed. The texture suggests concomitant fluo-

rapatite + calcite crystallization. Carbonate may also occur as faint veins cross-cutting the fluorapatite layers. Euhedral pyrochlore of about 200 μm in size was observed in sample HC559. Contacts between the fluorapatite + calcite layers and the carbonate matrix are sharp. Fluorapatite in sample HC34 occurs as flattened blebs up to 0.5 cm long, which often are interconnected to form irregular layers. The fluorapatite lenses of HC34 consist nearly exclusively of subhedral fluorapatite laths with a length between 100 and 300 μm. There are only a few small pockets of carbonate and some interspersed, euhedral pyrochlore crystals. The crystals are weakly aligned in what could be interpreted as a flow texture. For bulk analysis of the carbonate matrix, larger fluorapatite layers were cut out. The remaining carbonate matrix is calciocarbonatitic for all Homa samples (Table 1). The samples show an increase in Fe_2O_3(tot) and MgO from HC559 to HC554 to HC34 and a concomitant decrease in CaO.

The *Kalkfeld complex* is Cretaceous in age, and belongs to a group of geochemically very different magmatic complexes associated with the Damaraland magmatic province in northern Namibia (e.g., le Roex and Lanyon 1998). The samples were collected from the carbonatite which is spatially associated with silicate rocks of nephelinitic to phonolitic composition (Prins 1981). The widespread fenitization aureole (Bühn and Rankin 1999) suggests a shallow level of intrusion. The carbonatite consists of calciocarbonatites and ferrocarbonatites. From 11 samples analyzed, only 3 yielded reliable spot analyses of fluorapatite (KF50, KF59, KF94) because fluorapatite in the other samples is intimately intergrown with strontianite. The texture of these fluorapatite–strontianite intergrowths indicates late-stage crystallization. The fine-grained fluorapatites analyzed occur together with iron oxides as interstitial phases between coarse-grained calcite. Few pyrochlore crystals were observed in sample KF59. The samples classify as ferrocarbonatites after Woolley and Kempe (1989) on a whole rock basis, but the carbonate mineral is exclusively calcite, and the high iron contents derive from interstitial iron oxides. They are therefore classified as calciocarbonatites. The whole rock samples are rich in REE and Sr (Table 1), and have an apatite content between 2.5 and 13.5 wt% as determined by quantitative X-ray diffraction (XRD) analysis.

The *Ondurakorume complex* is located close to the Kalkfeld complex in northern Namibia. Again, a suite of carbonatitic rocks and associated silicate rocks is exposed (Prins 1981). In contrast to Kalkfeld, magnesiocarbonatite varieties with up to 13 wt% MgO are exposed at Ondurakorume, in addition to ferrocarbonatites and calciocarbonatites. The magnesiocarbonatites bear two carbonate minerals, of which one is calcite, and the other is a Ca–Mg–Fe carbonate with about 13 wt% MgO and 7 wt% FeO. Pyrochlore is present in places. The magnesiocarbonatites have only very little fluorapatite so that a continuous data set of fluorapatite compositions in calciocarbonatites, ferrocarbonatites, and magnesiocarbonatites could not be recovered. From the remaining six initially selected calciocarbonatite and ferrocarbonatite samples, five turned out to be unsuitable for fluorapatite analysis because this late-stage fluorapatite is intergrown with strontianite on the micrometer scale. The remaining sample ON76 has a calciocarbonatitic whole rock composition bearing micrometer-sized fluorapatite as an interstitial phase between calcite crystals. No pyrochlore was observed in that sample. The apatite content (Table 1) was determined at 14.3 wt% by XRD.

The *Otjisazu complex* in central Namibia has a very different genetic setting to the previous intrusions, and its lithologies compare with those described from the Phalaborwa complex, South Africa (Eriksson 1989). The Otjisazu complex has a Pan-African intrusion age, and represents a deeply eroded carbonatite body crystallized at 5–6 kbar (Bühn et al. 2001). It was selected for comparison with the shallow-level carbonatite centers described above. The circular intrusion consists of a central, main calciocarbonatite body with wollastonite-rich silicate rocks, rimmed by calcitic clinopyroxenites and then by clinopyroxenites. The latter bear lensoid calciocarbonatite bodies up to 500 m in length. The sequence of crystallization from pyroxenites with early calciocarbonatites through calcitic pyroxenites to late calciocarbonatites with silicate rocks at the base is treated as a cogenetic suite (Bühn et al. 2001). The pyroxenites are interpreted as cumulate rocks of a carbonatite magma (cf. Eriksson et al. 1985), representing the earliest stage of carbonatite fractionation. Silicate rocks of syenitic composition are exposed in direct contact to the carbonatite sequence.

All samples of this sequence contain fluorapatite up to 1 mm in size, of which only crystals with a long axis between 200 and 700 μm were selected for analysis. Sample OS87 is a pyroxenite consisting predominantly of clinopyroxene, and minor amounts of fluorapatite (13.0 wt%, Table 1), titanite and andraditic garnet. The pyroxenite sample OS64 contains less titanite and 5.0 wt% fluorapatite. The early calciocarbonatite bodies in the clinopyroxenite (OS155) consist of calcite, fluorapatite, and little clinopyroxene and andraditic garnet. Although their mineral content and major element composition is very similar to the central calciocarbonatite body, they have much lower concentrations of F, Ba, Sr, Y, and REE (Table 1), which suggests that they represent early calciocarbonatites in contrast to the central calciocarbonatite body. An intermediate member between the pyroxenites and the central calciocarbonatite is sample OS67, consisting of 80 wt% calcite, 10–20 wt% clinopyroxene, 4.4 wt% fluorapatite, and titanite. Accordingly, this sample has a very different major element composition to the pyroxenites, and is rich in Sr and REE. Sample OS69 is a silicate lens in the lower portion of the central calciocarbonatite. The sample consists mainly of wollastonite (about 50 vol%), the rest being largely clinopyroxene and andraditic garnet. Fluorapatite is an accessory phase with an abundance of less than 4 wt%. The Sr and REE abundances in the whole rock are comparable to that of the pyroxenites. A sample of the central main calciocarbonatite body is OS95, consisting mainly of calcite and fluorapatite (8.3 wt%), and clinopyroxene as an accessory phase in places. The sample has by far the highest content of Sr and REE. The $(Eu/Eu^*)_{cn}$ ratio in the whole rocks is slightly below unity for most samples.

Samples of the *North Ruri* carbonatite in west Kenya (Le Bas 1977) are from the Le Bas collection at The Natural History Museum, London. Sample N602 is an individual sample from that complex and has a calciocarbonatitic composition (Table 1). It shows a brecciated pure fluorapatite layer about 1 cm thick in a carbonate matrix. The fluorapatite occurs as subhedral laths below 100 μm in length, well aligned in a flow texture. Only a small amount of carbonate is observed in the fluorapatite layers, but calcite occurs in cross-cutting veins.

The *Okorusu carbonatite* belongs to the same group of carbonatites in northern Namibia as the Ondurakorume and Kalkfeld complexes. The sample OK8 does not derive from the carbonatite itself, but was collected from a fluorite–fluorapatite mineralization in marly country rocks adjacent to the carbonatite. The samples was analyzed to investigate fluorapatites crystallized from an undoubtedly late-stage carbonatitic fluid which invaded the country rocks. The fluorapatite forms prismatic euhedral crystals between 0.2 and 1.0 mm in size set in a matrix of fluorite + quartz. Because the host rock is not a carbonatite, no whole rock analysis was performed.

Analytical methods

Powdered whole rock carbonatite samples were analyzed for major elements on fusion tablets with a Philips PW 1400 XRF. The machine uses a Rh X-ray tube run at 40 kV accelerating voltage and 65 nA. The H_2O and CO_2 contents were determined by colorimetric titration. For Fe^{2+} analyses, aliquots of the powdered samples were decomposed in $HF–H_2SO_4$ and titrated with $KMnO_4$. The halogen concentration was determined by pyrohydrolytic means using Cl- and F-sensitive electrodes. Strontium, Y, and the REE were determined by ICP-MS (see Dulski 1994, for details) at the GFZ Potsdam. The Sr values of sample OS95 derives from XRF analysis after calibration against synthetic $CaCO_3–SrCO_3$ mixtures. Quantification of XRD analyses (Emmermann and Lauterjung 1990) was performed to approximate the weight percentage of apatite in the whole rocks.

Table 1 Whole rock composition of carbonatite and pyroxenite samples. *px* pyroxenite; *px/cb* mixed pyroxenite/carbonatite, *Si-cb* Si–rich lens in calciocarbonatite; *cb* calciocarbonatite. Major elements by XRF. Sr by ICP-MS for OS67, OS69, OS155, KF94, and ON76, for others by XRF. Y by XRF for HC34, HC554, HC559, and N602. Y and REE by ICP-AES for OS87, OS64, and KF59, for others by ICP-MS. Analyses OS67, OS69, OS95, and OS155 from Bühn et al. (2001)

Sample	OS87	OS64	OS155	OS67	OS69	OS95	KF50	KF59	KF94	ON76	HC34	HC554	HC559	N602
Rock type	px	px	cb	px/cb	Si-cb	cb	cb	cb	cb	cb	cb	cb	cb	cb
wt%														
SiO_2	43.1	45.4	2.77	9.98	47.6	5.59	1.85	0.12	2.82	1.23	0.87	0.08	1.29	0.53
TiO_2	0.81	3.77	0.24	0.47	0.36	0.05	0.05	0.04	0.49	0.07	0.13	0.07	0.17	0.09
$A1_2O_3$	3.42	2.75	0.89	0.90	1.15	1.85	0.49	0.34	0.99	0.58	0.29	0.29	0.69	0.42
Fe_2O_3	5.96	6.23	1.90	1.10	2.22	b.d.	6.60	2.50	7.71	5.05	5.97	3.07	2.76	5.74
FeO	5.68	6.86	0.99	1.73	2.52	0.14	0.34	0.09	0.23	0.28	–	–	–	–
MnO	0.41	0.43	0.08	0.13	0.53	0.07	1.78	1.67	1.96	1.75	0.74	0.49	0.39	1.34
MgO	7.48	6.95	0.81	1.57	2.29	0.09	2.51	0.76	0.44	1.11	0.63	0.40	0.27	0.68
CaO	24.5	21.9	47.7	43.8	39.6	44.9	32.5	38.4	39.9	42.1	42.3	46.7	48.4	43.0
Na_2O	1.89	1.84	0.09	0.53	0.76	0.67	0.07	0.12	0.04	b.d.	0.32	0.78	0.04	0.11
K_2O	0.12	0.02	0.05	b.d.	0.02	0.35	0.04	0.01	0.12	0.04	0.04	0.04	0.01	0.12
P_2O_5	4.96	1.62	2.52	1.79	1.04	3.47	0.98	4.99	3.99	5.43	1.53	7.70	0.30	0.7
H_2O	0.33	0.31	0.53	0.27	0.25	0.36	1.1	0.6	1.4	1.2	–	–	–	–
CO_2	0.11	0.15	40.4	33.7	0.33	36.8	44.2	42.7	35.6	35.7	–	–	–	–
ppm														
F	2,300	1,350	660	890	530	1,700	4,200	4,400	2,600	4,100	–	–	–	–
Cl	<100	<100	<100	<100	<100	<100	–	<100	<100	<100	–	–	–	–
Sr	1,445	751	7,075	12,892	1,025	2.2%	3.7%	4.2%	6,182	25,858	2,990	5,780	2,310	3,070
Y	85	125	95.3	104	115	140	137	738	504	268	280	400	60	140
La	364	330	352	581	372	1,047	5,623	3,932	4,384	1,922	–	–	–	–
Ce	873	850	734	1,148	760	2,014	10,112	7,492	8,006	4,056	–	–	–	–
Pr	120	133	92.8	136	93.3	232	1,050	744	849	488	–	–	–	–
Nd	391	419	343	490	323	813	3,006	2,520	2,570	1,696	–	–	–	–
Sm	72.5	75	57.0	75.3	53.1	118	341	369	314	238	–	–	–	–
Eu	17.1	20	14.4	17.8	11.3	25.9	83.5	101	87.3	63.6	–	–	–	–
Gd	41.8	26	41.6	53.8	38.0	77.5	155	269	205	141	–	–	–	–
Tb	–	–	4.74	5.74	4.64	7.98	11.5	36	25.1	15.5	–	–	–	–
Dy	22.1	42	22.3	25.4	22.0	34.8	34.7	188	115.5	70.1	–	–	–	–
Ho	2.78	4.6	3.61	3.85	3.63	5.24	5.07	29	19.2	10.7	–	–	–	–
Er	5.15	9.7	7.93	8.27	8.73	10.6	11.1	60	43.2	21.7	–	–	–	–
Tm	–	–	0.86	0.94	1.18	1.15	1.53	–	4.91	2.29	–	–	–	–
Yb	3.98	4.4	4.95	4.99	6.88	5.39	10.2	30	23.4	10.58	–	–	–	–
Lu	0.65	0.8	0.67	0.78	1.05	0.83	2.16	–	3.23	1.43	–	–	–	–
Total	99.3	98.7	99.9	97.6	99.1	97.2	98.7	98.6	98.3	98.4	53.1	60.2	54.6	53.1
Fe^{3+}/Fe^{2+}	0.94	0.82	1.73	0.57	0.79	–	17.5	25.0	30.2	16.2	–	–	–	–
REE (ppm)	1,914	1,915	1,680	2,552	1,699	4,393	20,447	15,770	16,650	8,737	–	–	–	–
Y/Ho	30.6	27.2	26.4	27.0	31.7	26.7	27.0	25.4	26.3	25.0	–	–	–	–
(La/Nd)cn	1.8	1.5	2.0	2.3	2.2	2.5	3.6	3.0	3.3	2.2	–	–	–	–
(La/Yb)cn	63	52	49	81	37	134	382	91	130	126	–	–	–	–
(Eu/Eu*)cn	0.94	1.38	0.90	0.85	0.76	0.82	1.10	0.97	1.04	1.05	–	–	–	–
Apatite (wt%)	13.0	5.0	6.6	4.4	<4.0	8.3	2.5	11.3	13.5	14.3	–	–	–	–

Individual fluorapatite crystals were analyzed with a Cameca SX50 microprobe on doubly polished wafers between 90 and 150 μm thick. A possible chemical zonation on the micrometer scale as observed in apatite (e.g., Tepper and Kuehner 1999) was overcome by a defocused microprobe beam of 20×20 μm. An accelerating voltage of 15 kV at 20 nA beam current was applied for analysis of F, Na, S, Mn, and Ce. Calibration was done against natural albite (Na), synthetic barite (S), natural spessartine (Mn), and synthetic CeAl. Sodium, Mn, and S were detected via K-shell excitation at 20 s counting time on the peak and 10 s on the background. Analysis for F in fluorapatite generally faces problems in an accurate determination of the F–Kα X-ray peak, and because of diffusion effects of F towards the sample surface (Stormer et al. 1993). A comparison between standardizations against fluorapatite, LaF_3, CaF_2, and PbF_2 with a TAP crystal indicates that the CaF_2 standard yields the most reliable results for fluorine analysis. The fluorite standard yielded a precision of $< 5\%$, at a counting time of 15 s on the peak. The calibration, however, overestimated the F concentration in a fluorapatite standard (F = 3.70 wt%) by 15%, which is likely due to the diffusion effects of F (Stormer et al. 1993). A similar deviation may be considered for the fluorapatite analyses presented here. A PET crystal was used to measure L-shell fluorescence lines of Ce at 30 s counting time on the peak, and 15 s counting time each on the upper and lower backgrounds. A fluorapatite standard yielded results within 11.5% relative error for Ce, which is used as an internal standard element for the quantification of synchrotron-XRF spectra.

The wafers were then dismounted from the glass plate for synchrotron micro-XRF analysis at beam line L of the Hamburg Synchrotron Laboratory (HASYLAB) at the Deutsches Elektronen Synchrotron (DESY), Germany. An elliptically shaped glass capillary was used to focus the incident beam to a 20 μm diameter. Trace element determinations were performed on exactly the same spots as analyzed by electron microprobe. The choice of wafer thickness and beam diameter relative to the fluorapatite crystal size ensured that no neighboring minerals affected the acquired fluorapatite spectra, and that effects of possible chemical zonations were minimized. The white spectrum of the beam allowed simultaneous detection of Sr, Y, Ba, and REE K-shell fluorescence lines, and L-shell fluorescence lines of Th (see Bühn et al. 1999). Long-time measurements between 1,800 and 3,600 s lifetime were taken on the spots, inserting an 8 mm aluminum absorber between the source and the sample to reduce the dead time. The quantification of the synchrotron-XRF spectra is based on fundamental parameter analysis (Vincze 1995). A fluorapatite density of 3.2 g/cm^3 and a O–P–Ca fluorapatite matrix were used for the z-dependent correction for absorption of fluorescence. As an internal standard, the Ce determinations of the electron microprobe were used, because Ce has the highest concentration within the group of REE for all fluorapatites. The preference was given to Ce instead of lighter elements of higher concentration in fluorapatites (Ca, P), because errors in the determination of wafer thickness, mineral density, absorber thickness and fluorapatite matrix have a much higher effect on the quantification of Y and the REE for light elements than for Ce. With Ce as a reference element, a 10% relative error in fluorapatite density results in a 2% relative error for Y determinations. A 10% relative error in the determination of the wafer thickness yields a 2.5% relative error for Y. For the HREE, a relative error on fluorapatite density or wafer thickness of 10% each would lead to a 3.5% relative error for Yb determinations. The relatively light matrix of fluorapatite has a negligible influence on element determinations of high atomic weight as those analyzed here.

A cross-check with laser ablation ICP-MS data using a VG PlasmaQuad 3 at The Natural History Museum, London, was performed for two selected fluorapatite samples OS67 (convex-upward REE pattern) and OK8 (straight REE pattern). The relative errors were mostly $< 20\%$ for Y, La, and Dy, but reached higher values for individual analyses. The ICP-MS data, however, are all within the compositional range of the synchrotron-XRF analyses, so that the deviation is probably due to heterogeneities in individual crystals. All laser ablation ICP-MS data clearly reproduce the different shapes of the REE patterns of the two samples.

Results

Rare-earth element and Y composition of fluorapatites

In spite of the high REE content of the Kalkfeld and Ondurakorume bulk samples in comparison to all other bulk rocks (Table 1), their fluorapatites are relatively poor in La and REE (Table 2) and have a convex-upward REE pattern (Fig. 2). Sample KF50 fluorapatites have REE patterns with $(La/Nd)_{cn} = 0.7$ (peaking at Nd–Sm), KF59 has $(La/Nd)_{cn} = 0.6$ (peaking also at Nd–Sm), and KF94 fluorapatites have $(La/Nd)_{cn} = 1.0$ peaking at Pr. ON76 fluorapatites have $(La/Nd)_{cn}$ at 0.8 with patterns peaking between Nd and Sm. Like the literature fluorapatite data (Fig. 1), the Kalkfeld and Ondurakorume fluorapatites display a positive correlation between the ratio $(La/Yb)_{cn,}$ and the La_{cn} content and $(La/Nd)_{cn}$ (Fig. 3). The Y concentrations decrease as $(La/Yb)_{cn}$ increases. The Y/Ho ratios vary between 18 and 55 for all analyses performed (Table 2) and therefore, in parts, significantly deviate from the chondritic value of 28 after Anders and Grevesse (1989). Some analyses of ON76 display a slight negative $(Ce/Ce^*)_{cn}$ anomaly (Fig. 2).

Similar relationships are observed for the Homa samples. The ratios $(La/Nd)_{cn}$ and $(La/Yb)_{cn}$ increase with increasing La in fluorapatite from 450 over 741 to 1,637 ppm (Table 4). As La and ΣREE increase, the REE patterns develop from a distinctly convex-upward shape with $(La/Nd)_{cn} < 1$ in sample HC559 to a flat pattern (HC554) and then a straight REE pattern in HC34 with a negative slope throughout (Fig. 2). Consequently, there is a clear positive correlation between $(La/Nd)_{cn}$ and $(La/Yb)_{cn}$ for all Homa analyses (Fig. 3). The convex-upward shaped REE patterns at Homa peak at Sm–Eu. Again, there is a positive correlation between the La_{cn} content and the $(La/Yb)_{cn}$ ratio, and a negative $(Eu/Eu^*)_{cn}$ anomaly develops from 1.0 in HC559 to 0.8 in HC34 as the ratio $(La/Yb)_{cn}$ increases (Fig. 3). The Y concentrations decrease as $(La/Yb)_{cn}$ increases. A negative $(Ce/Ce^*)_{cn}$ anomaly is developed in the low-REE samples HC559 and HC554 (Table 4) which reaches 0.4 in one analysis, while sample HC34 with the highest La content and $(La/Yb)_{cn}$ ratio displays no Ce anomaly.

The ΣREE and La contents of the Otjisazu fluorapatites increase from clinopyroxenites (OS87, OS64), to the clinopyroxenite/calciocarbonatite sample OS67 towards fluorapatites in OS69 and OS95 of the central calciocarbonatite (Table 3). While samples OS87 and OS64 have La below 0.1 wt%, $(La/Yb)_{cn}$ around 20, and $(La/Nd)_{cn} < 1$, the fluorapatites OS69 and OS95 of the central calciocarbonatite sequence have high La contents, $(La/Nd)_{cn} > 2$ and high $(La/Yb)_{cn}$ ratios between 180 and 250. Accordingly, fluorapatites with a convex-

Table 2 Composition of carbonatitic fluorapatites – Ondurakorume and Kalkfeld. *n* mean value of *n* analyses, *SD* 1 sigma standard deviation. Major elements and Ce by electron microprobe, trace elements by synchrotron micro-XRF. *Eu** $(Eu/Eu^*)_{cn}$, *Ce** $(Ce/Ce^*)_{cn}$. La/Nd and La/Yb ratios chondrite-normalized

	ON76				KF50			KF59				KF94			
	1	2	$n=6$	SD	1	2	$n=2$	1	2	$n=4$	SD	1	2	$n=6$	SD
wt%															
P_2O_5	39.8	39.3	39.4	0.2	40.1	39.9	40.0	40.0	39.6	39.8	0.1	38.6	38.2	38.3	0.1
SiO_2	0.07	0.04	0.05	0.02	0.04	0.09	0.07	0.06	0.00	0.01	0.02	2.90	0.94	1.76	0.62
CaO	52.2	52.4	52.2	0.2	52.9	52.6	52.8	51.9	51.7	51.9	0.2	50.3	51.9	51.3	0.5
MnO	0.08	0.04	0.07	0.02	0.04	0.10	0.07	0.15	0.19	0.14	0.06	0.08	0.00	0.23	0.20
Na_2O	0.44	0.40	0.43	0.08	0.43	0.39	0.41	0.45	0.49	0.44	0.03	0.20	0.27	0.24	0.02
SO_3	0.15	0.01	0.07	0.05	0.00	0.08	0.04	0.04	0.04	0.05	0.01	0.08	0.06	0.05	0.02
F	3.5	3.7	3.7	0.1	3.4	3.6	3.5	3.1	4.1	3.5	0.3	3.7	4.3	3.8	0.2
–O = F	1.5	1.6	1.6	–	1.4	1.5	1.5	1.3	1.7	1.5	–	1.6	1.8	1.6	–
ppm															
Sr	16,750	13,119	15,090	1,170	10,820	9,136	9,978	9,466	9,670	10,204	1,670	13,250	11,860	11,636	1,012
Y	1,071	1,028	1,122	110	1,974	1,202	1,588	3,367	3,005	3,048	216	1,416	1,036	1,203	119
Ba	2,528	8,532	5,547	2,232	148	326	237	76	276	146	71	128	119	137	14
La	952	748	873	102	541	489	515	515	715	581	75	1,187	1,098	1,100	50
Ce	2,900	2,100	2,841	342	2,000	1,400	1,700	1,900	2,400	1,997	252	3,300	3,000	3,146	106
Pr	512	348	441	76	326	209	268	315	430	340	52	493	435	475	22
Nd	2,621	1,798	2,244	407	1,825	1,175	1,500	1,926	2,347	1,952	233	2,309	2,049	2,232	101
Sm	666	426	546	108	624	386	505	616	708	601	68	531	457	506	27
Eu	169	101	134	31	206	125	166	180	217	178	23	143	116	132	9
Gd	499	309	399	82	680	407	544	611	681	580	68	381	326	362	20
Tb	60	39	46	7	77	50	63	81	91	77	9	46	37	41	3
Dy	370	309	304	39	418	250	334	586	620	537	63	261	193	225	21
Ho	53	60	46	11	39	26	33	77	76	67	9	33	24	28	3
Er	98	81	80	12	108	66	87	216	230	194	28	97	72	80	9
Tm	–	–	–	–	11	9	10	–	–	–	–	14	11	12	1
Yb	42	34	35	7	54	39	46	90	108	87	14	67	42	50	9
Lu	–	–	–	–	7	7	7	17	18	14	3	12	9	10	1
Th	238	557	414	112	529	313	421	117	344	185	83	132	125	131	4
Total	97.7	97.3	97.3	–	97.5	96.8	97.2	96.4	96.6	96.4	–	96.7	96.0	96.2	–
REE	8,942	6,353	7,989	1,223	6,917	4,637	5,777	7,117	8,641	7,203	898	8,874	7,866	8,397	381
La/Nd	0.70	0.80	0.76	0.06	0.57	0.80	0.66	0.52	0.59	0.57	0.03	0.99	1.03	0.95	0.06
La/Yb	15.5	15.2	17.9	2.8	6.9	8.8	7.7	4.0	4.6	4.7	0.4	12.3	18.1	15.7	2.0
Eu*	0.89	0.85	0.87	0.03	0.96	0.96	0.96	0.89	0.95	0.91	0.02	0.97	0.91	0.93	0.02
Ce*	1.00	1.01	1.11	0.15	1.14	1.05	1.10	1.11	1.05	1.08	0.02	1.04	1.04	1.04	0.01
Y/Ho	20.1	17.1	24.3	8.7	50.1	46.1	48.5	43.5	39.3	45.8	5.0	42.9	43.2	43.6	0.6

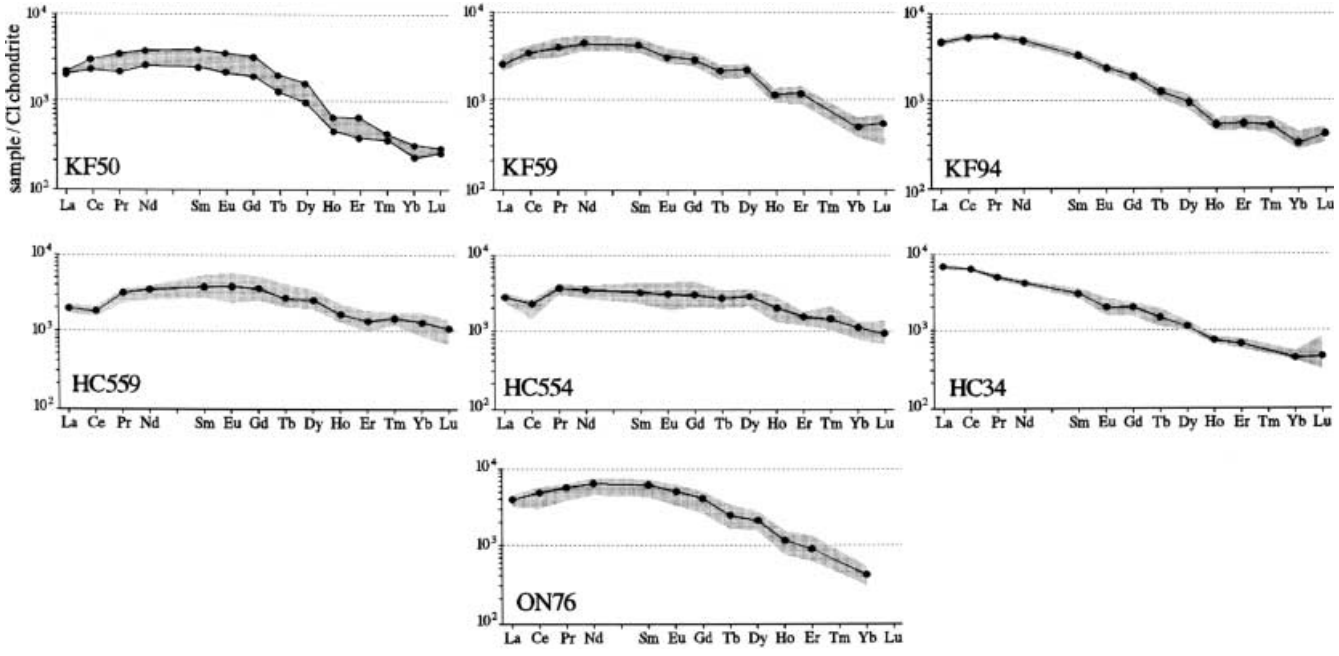

Fig. 2 REE distribution in fluorapatites from Kalkfeld, Homa Mountain, and Ondurakorume. The *shaded area* gives the compositional range of all analyses performed, *dots* are mean values (see Tables 2 and 4)

upward shaped REE pattern are confined to the clinopyroxenite sequence, while fluorapatite of the central calciocarbonatite sequence including the silicate lens OS69 has a steep, straight REE pattern. The intermediate pyroxenite/calciocarbonatite sample OS67 also has fluorapatite with an intermediate composition of 0.15 wt% La. Significantly, fluorapatites of the early calciocarbonatite body in the clinopyroxenites (OS155) have convex-upward shaped REE patterns, (La/

Fig. 3 Rare-earth element and Y characteristics of the carbonatitic fluorapatites analyzed. *First row* Kalkfeld and Ondurakorume, *second row* Homa Mountain, *third row* Otjisazu. KF50 *open triangles*, KF59 *small dots*, KF94 *stars*, ON76 *full squares*, HC34 *circles*, HC554 *pluses*, HC559 *short dashes*, OS87 *full diamonds*, OS64 *open squares*, OS67 *full triangles*, OS69 *crosses*, OS95 *open diamonds*, OS155 *small full squares*

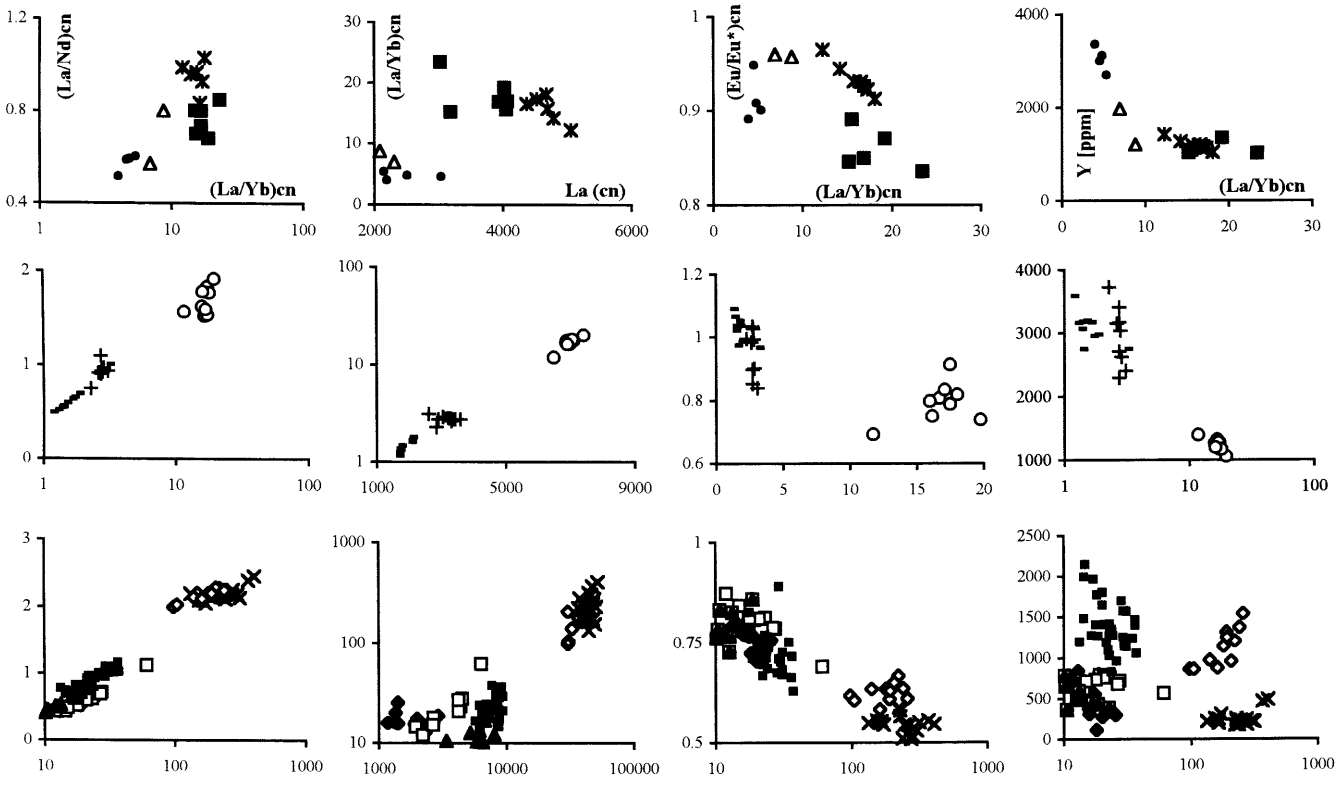

Table 3 Composition of carbonatitic fluorapatites – Otjisazu. *n* mean value of *n* analyses, *SD* 1 sigma standard deviation. Major elements and Ce by electron microprobe, trace elements by synchrotron micro-XRF. *Eu** $(Eu/Eu^*)_{cn}$, *Ce** $(Ce/Ce^*)_{cn}$. La/Nd and La/Yb ratios chondrite-normalized

	OS155				OS87				OS64				OS67				OS69				OS95			
	1	2	$n=33$	SD	1	2	$n=10$	SD	1	2	$n=10$	SD	1	2	$n=10$	SD	1	2	$n=18$	SD	1	2	$n=11$	SD
wt%																								
P_2O_5	39.9	39.3	39.3	0.4	40.9	40.1	40.5	0.4	38.4	38.8	38.9	0.5	39.4	38.3	39.1	0.4	37.2	36.9	37.3	1.0	38.2	36.1	37.3	1.3
SiO_2	0.55	0.79	0.66	0.07	0.45	0.69	0.47	0.11	0.67	0.86	0.76	0.13	0.95	0.98	0.90	0.08	2.87	2.92	2.94	0.76	0.93	1.56	1.19	0.26
CaO	52.6	52.6	52.3	0.3	53.7	53.0	53.4	0.2	54.2	53.0	53.5	0.4	52.6	52.0	52.3	0.2	49.7	49.1	49.2	0.3	50.1	48.7	49.5	0.4
MnO	0.03	0.03	0.02	0.01	0.00	0.00	0.01	0.01	0.02	0.04	0.04	0.04	0.00	0.04	0.02	0.02	0.00	0.00	0.01	0.02	0.02	0.00	0.01	0.00
Na_2O	0.09	0.10	0.01	0.01	0.13	0.08	0.11	0.02	0.06	0.05	0.08	0.02	0.11	0.11	0.10	0.03	0.12	0.13	0.15	0.16	0.28	0.29	0.29	0.02
SO_3	0.04	0.05	0.00	0.01	0.49	0.56	0.52	0.05	0.62	0.61	0.58	0.06	0.40	0.31	0.39	0.09	1.21	1.21	1.02	0.21	0.25	0.13	0.25	0.08
F	2.8	2.9	2.9	0.1	3.1	3.2	3.2	0.2	3.5	3.7	3.6	0.2	3.2	3.7	3.6	0.3	3.3	3.8	3.5	0.3	4.1	4.3	4.3	0.2
–O = F	1.2	1.2	1.2	–	1.3	1.3	1.3	–	1.5	1.6	1.5	–	1.3	1.6	1.5	–	1.4	1.6	1.5	–	1.7	1.8	1.8	–
ppm																								
Sr	8,785	13,700	17,031	4,764	3,835	7,534	6,396	1,744	4,637	6,095	5,438	572	3,605	6,828	5,737	1,211	3,230	4,888	4,719	1,279	18,560	28,070	20,865	3,911
Y	1,270	1,991	1,400	301	301	845	499	194	619	758	707	66	364	731	558	146	181	256	257	87	959	1,548	1,127	223
Ba	8	20	77	113	9	14	13	4	11	23	19	4	9	21	19	7	15	32	22	8	153	239	170	44
La	1,357	2,041	1,843	268	333	545	421	122	460	993	855	304	793	1,873	1,484	299	8,844	11,600	10,638	982	7,144	11,160	8,834	1,298
Ce	4,300	6,600	5,579	685	1,100	2,300	1,603	520	2,000	3,700	3,032	693	3,200	7,000	5,460	973	18,000	24,300	21,941	1,955	14,000	22,000	17,642	2,404
Pr	630	1,040	807	108	191	462	303	107	402	667	542	81	594	1,280	978	198	1,982	2,754	2,436	222	1,481	2,512	1,985	302
Nd	3,203	5,304	3,925	569	952	2,450	1,544	565	2,075	3,192	2,639	355	3,361	7,041	5,338	1,195	7,592	10,650	9,382	847	6,023	9,707	7,829	1,033
Sm	714	1,268	859	158	202	567	347	131	466	658	558	62	836	1,753	1,304	322	1,232	1,710	1,510	136	979	1,579	1,321	155
Eu	142	288	176	44	41	123	73	28	104	141	119	16	185	380	288	76	137	206	177	18	155	231	199	20
Gd	518	949	607	132	134	394	238	91	318	426	364	38	624	1,296	952	257	523	741	639	67	534	835	712	75
Tb	46	94	61	13	14	39	24	8	31	43	35	4	61	132	94	26	47	74	60	8	49	91	71	11
Dy	256	484	299	74	62	184	109	43	133	173	147	15	316	684	485	137	163	247	202	27	192	315	265	31
Ho	38	57	45	9	7	15	10	3	11	13	12	1	34	78	53	15	14	27	22	4	38	66	70	17
Er	99	160	110	24	17	51	31	12	38	49	43	3	97	204	145	39	42	64	56	8	74	119	116	19
Tm	–	–	–	–	–	–	–	–	–	–	–	–	4	13	7	3	6	13	9	6	–	–	–	–
Yb	50	98	56	15	9	29	17	6	22	33	26	4	52	107	78	19	22	52	33	10	24	30	36	8
Lu	14	16	13	5	3	5	4	1	4	6	5	1	9	17	15	5	0	15	9	10	2	13	4	4
Th	446	666	564	139	220	388	244	84	273	369	358	40	98	220	173	36	627	995	905	238	442	657	490	98
Total	97.0	97.9	97.3	–	98.2	97.9	98.0	–	97.1	97.2	97.4	–	96.7	96.9	97.2	–	97.3	98.4	97.9	–	97.3	97.2	97.2	–
REE	11,370	18,398	14,381	2,105	3,065	7,164	4,723	1,637	6,064	10,094	8,377	1,576	10,166	21,858	16,678	3,563	38,604	52,453	47,114	4,300	30,697	48,658	39,086	5,374
La/Nd	0.82	0.74	0.91	0.13	0.67	0.43	0.54	0.07	0.43	0.60	0.62	0.19	0.45	0.51	0.55	0.13	2.25	2.10	2.19	0.10	2.29	2.22	2.17	0.09
La/Yb	18.8	14.5	24.1	6.7	25.6	13.0	17.5	3.3	14.5	20.8	23.8	13.4	10.6	12.1	13.8	4.0	278	154	245	73	206	258	181	49.2
Eu*	0.71	0.80	0.73	0.05	0.76	0.79	0.76	0.02	0.82	0.81	0.80	0.05	0.78	0.77	0.78	0.04	0.52	0.56	0.55	0.02	0.65	0.61	0.63	0.02
Ce*	1.12	1.09	1.10	0.03	1.05	1.10	1.08	0.01	1.11	1.09	1.08	0.02	1.12	1.08	1.09	0.03	1.03	1.03	1.03	0.01	1.03	1.00	1.01	002
Y/Ho	33.2	34.7	30.8	5.5	43.0	56.3	51.9	4.3	56.3	58.3	58.4	6.7	10.7	9.4	10.7	1.4	12.9	9.5	11.9	2.9	25.2	23.5	16.0	5.7

Table 4 Composition of carbonatitic fluorapatites – Homa, North Ruri, and Okorusu. *n* mean value of *n* analyses, *SD* 1 sigma standard deviation. Major elements and Ce by electron microprobe, trace elements by synchrotron micro-XRF. *Eu** $(Eu/Eu^*)_{cn}$, *Ce** $(Ce/Ce^*)_{cn}$. La/Nd and La/Yb ratios chondrite-normalized

	HC34				HC554				HC559				N602				OK8			
	1	2	$n=9$	SD	1	2	$n=9$	SD	1	2	$n=10$	SD	1	2	$n=11$	SD	1	2	$n=9$	SD
wt%																				
P_2O_5	39.2	38.4	39.0	0.7	35.5	34.6	35.7	0.6	35.1	37.3	36.6	1.0	38.8	38.8	37.8	0.8	39.6	39.6	39.7	0.1
SiO_2	0.10	0.08	0.09	0.03	0.00	0.00	0.00	0.00	0.14	0.12	0.13	0.01	0.00	0.02	0.01	0.01	0.42	0.27	0.32	0.05
CaO	50.9	50.2	51.2	0.6	51.7	51.5	51.0	0.5	50.0	46.4	48.1	0.9	50.4	50.9	50.9	0.2	52.2	52.9	52.6	0.2
MnO	0.15	0.14	0.11	0.04	0.03	0.13	0.16	0.10	0.25	0.24	0.21	0.04	0.15	0.13	0.11	0.03	0.00	0.00	0.01	0.01
Na_2O	1.14	1.43	0.95	0.33	3.74	3.52	3.27	0.32	4.24	4.05	4.05	0.10	0.61	0.49	0.50	0.05	0.11	0.08	0.10	0.01
SO_3	0.04	0.03	0.03	0.01	0.19	0.22	0.20	0.03	0.18	0.34	0.28	0.04	0.03	0.00	0.02	0.01	0.00	0.03	0.02	0.01
F	4.3	4.4	4.4	0.4	2.9	3.9	3.1	0.4	3.2	4.0	3.7	0.3	4.5	4.9	4.8	0.2	4.1	4.3	4.1	0.1
–O=F	1.8	1.9	1.9	–	1.2	1.6	1.3	–	1.3	1.7	1.6	–	1.9	2.1	2.0	–	1.7	1.8	1.7	–
ppm																				
Sr	17,090	19,370	18,431	1,665	30,533	41,981	37,669	3,354	34,060	41,202	29,161	9,122	15,930	16,300	16,648	483	13,840	10,440	10,389	2,282
Y	1,057	1,319	1,235	93	2,404	3,403	2,946	448	2,743	3,585	3,078	234	307	353	321	14	196	137	143	32
Ba	1,844	3,123	2,739	560	2,581	2,822	2,668	203	2,062	2,802	1,961	511	175	192	242	50	82	88	75	12
La	1,743	1,616	1,637	54	613	802	741	71	388	381	450	103	5,454	5,856	5,832	173	2,363	1,826	2,057	154
Ce	3,800	3,700	3,689	88	1,200	1,400	1,372	231	1,100	900	1,148	194	8,200	8,900	8,666	183	4,400	3,400	3,880	278
Pr	405	447	431	24	283	390	340	32	235	261	246	10	655	833	714	58	401	328	377	25
Nd	1,753	2,050	1,884	131	1,265	1,712	1,550	146	1,359	1,492	1,392	52	2,184	2,541	2,333	93	1,421	1,104	1,288	94
Sm	389	531	458	58	355	492	465	76	541	658	571	38	367	451	383	32	197	156	187	18
Eu	84	128	110	21	108	188	165	38	205	267	215	24	70	67	66	2	35	24	30	3
Gd	307	437	379	51	427	618	587	111	669	842	709	64	210	225	195	20	91	65	82	9
Tb	40	62	54	10	71	100	98	16	97	126	104	9	20	30	23	3	10	8	10	1
Dy	243	342	292	33	509	717	694	103	609	750	639	49	84	90	78	8	31	26	31	4
Ho	35	44	41	4	70	103	109	24	78	101	87	7	31	32	33	1	9	6	7	1
Er	84	108	102	10	179	267	251	33	202	242	212	13	67	78	60	11	20	13	19	4
Tm	–	–	–	–	25	38	36	8	34	37	34	2	–	–	–	–	–	–	–	–
Yb	61	67	69	8	137	203	189	23	197	230	199	16	14	23	15	4	4	7	9	4
Lu	11	5	11	4	19	23	24	5	30	27	26	3	0	6	4	2	5	2	3	1
Th	1,134	1,199	1,345	132	347	518	395	83	183	297	221	32	183	226	245	36	706	486	520	109
Total	97.0	96.3	97.2	–	97.0	97.8	97.1	–	96.2	96.1	95.6	–	96.0	96.9	95.8	–	97.1	97.2	97.0	–
REE	8,955	9,537	9,155	497	5,262	7,053	6,618	916	5,746	6,313	6,031	586	17,356	19,132	18,402	590	8,987	6,965	7,980	596
La/Nd	1.92	1.52	1.68	0.14	0.93	0.90	0.93	0.08	0.55	0.49	0.62	0.14	4.81	4.44	4.82	0.21	3.19	3.21	3.08	0.13
La/Yb	19.8	16.7	16.7	2.1	3.1	2.7	2.7	0.2	1.4	1.1	1.6	0.5	270	176	277	66	181	409	200	100
Eu*	0.74	0.81	0.79	0.06	0.84	1.03	0.95	0.07	1.03	1.09	1.03	0.04	0.77	0.64	0.74	0.06	0.72	0.79	0.73	0.04
Ce*	1.08	1.04	1.05	0.02	0.72	0.62	0.66	0.10	0.85	0.71	0.83	0.05	1.04	0.97	1.02	0.03	1.05	1.08	1.06	0.02
Y/Ho	30.2	30.0	30.3	1.6	34.3	33.1	27.1	6.0	35.0	35.4	35.4	0.2	9.9	11.0	9.8	0.7	21.8	22.8	19.8	3.0

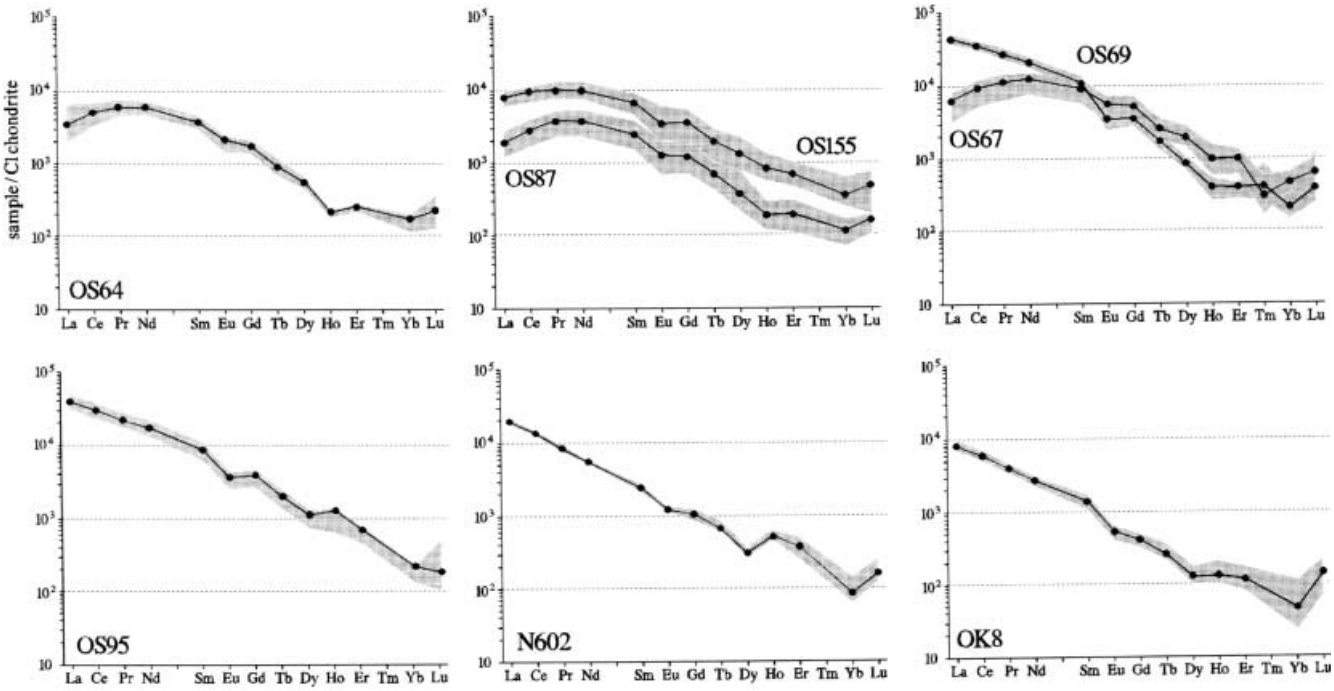

Fig. 4 REE distribution in fluorapatites from Otjisazu, North Ruri, and Okorusu. *Dots* represent mean values

$Nd)_{cn} < 1$, and low $(La/Yb)_{cn}$ ratios of 14–19 (Table 3), and are therefore distinctly different from fluorapatites of the central calciocarbonatite (OS95). All fluorapatite REE patterns with $(La/Nd)_{cn} < 1$ peak at Nd (Fig. 4). There is again a positive correlation between the ratio $(La/Yb)_{cn}$, and the La_{cn} content and $(La/Nd)_{cn}$ ratio (Fig. 3). As $(La/Yb)_{cn}$ increases from pyroxenitic fluorapatites towards fluorapatites of the central calciocarbonatite, $(Eu/Eu^*)_{cn}$ develops from only a weak negative to a distinctly negative anomaly. The Y concentrations in the fluorapatites display a largely decreasing trend as $(La/Yb)_{cn}$ increases, but the central calciocarbonatite sample OS95 bears high-Y fluorapatite. The Y/Ho ratios greatly vary from 40–75 in pyroxenitic to 10–25 in central calciocarbonatite fluorapatites (Table 3). Sample OS67 has the lowest Y/Ho ratios in fluorapatite, consistently close to 10.

The fluorapatites of the North Ruri carbonatite N602 have relatively high La contents of 0.6 wt% La (Table 4). From the previous relationships observed, it can be expected that their REE patterns are straight, have high $(La/Nd)_{cn}$ and $(La/Yb)_{cn}$ ratios, display a negative $(Eu/Eu^*)_{cn}$ anomaly, and have low Y concentrations. Indeed, they plot on a straight line (Fig. 4), and have $(La/Nd)_{cn} = 4.8$ and $(La/Yb)_{cn} = 277$. They display a distinct negative $(Eu/Eu^*)_{cn}$ anomaly at 0.74, and have low Y concentrations of about 300 ppm, and Y/Ho ratios far below the chondritic ratio of 28 (Table 4). Although the OK8 fluorapatites crystallized from late-stage carbonatitic fluid have moderate La contents of 2,000 ppm (Table 4), they display straight REE patterns (Fig. 4) with high $(La/Yb)_{cn}$ ratios of 200, and a distinct $(Eu/Eu^*)_{cn}$ anomaly of 0.73. The Y concentrations are very low (below 200 ppm), and the Y/Ho ratios are again below the chondritic value of 28.

Other elements

Some fluorapatite analyses yielded F contents significantly above the stoichiometric value of 3.77 wt% F (Tables 2, 3, 4). High F contents in fluorapatites are known to correlate with CO_2 contents in the percentage range (Binder and Troll 1989; Regnier et al. 1994; Nathan 1996) testifying to a carbonate-fluorapatite composition. There is a weak negative correlation of $R = -0.33$ between the F contents and the analysis totals for our analyses, which suggests that high-F fluorapatites also contain components not analyzed (CO_2, OH, Cl). Within the carbonatite suites, for example at Homa and at Otjisazu, the F contents in fluorapatites are positively correlated with ΣREE as also found for fluorapatites of the Kovdor carbonatite, Russia (Zaitsev and Bell 1995). A positive correlation for the entire data set is also seen between the F contents, and the $(La/Nd)_{cn}$ and $(La/Yb)_{cn}$ ratios ($R = 0.67$ and $R = 0.47$, respectively).

The Sr distribution does not display a consistent pattern. The high-La sample OS95 contains the highest Sr concentration of the Otjisazu sequence, but the high-La sample HC34 of the Homa sequence contains the least Sr concentration in that suite (Tables 3 and 4). Also, there is no significant difference in Sr contents between the low-La fluorapatites of Ondurakorume and Kalkfeld, and the high-La samples OK8 and N602. However, there is a weak positive correlation between the Sr and the Y content in the fluorapatites (Fig. 5a), and the $(Eu/Eu^*)_{cn}$ anomaly largely correlates with the

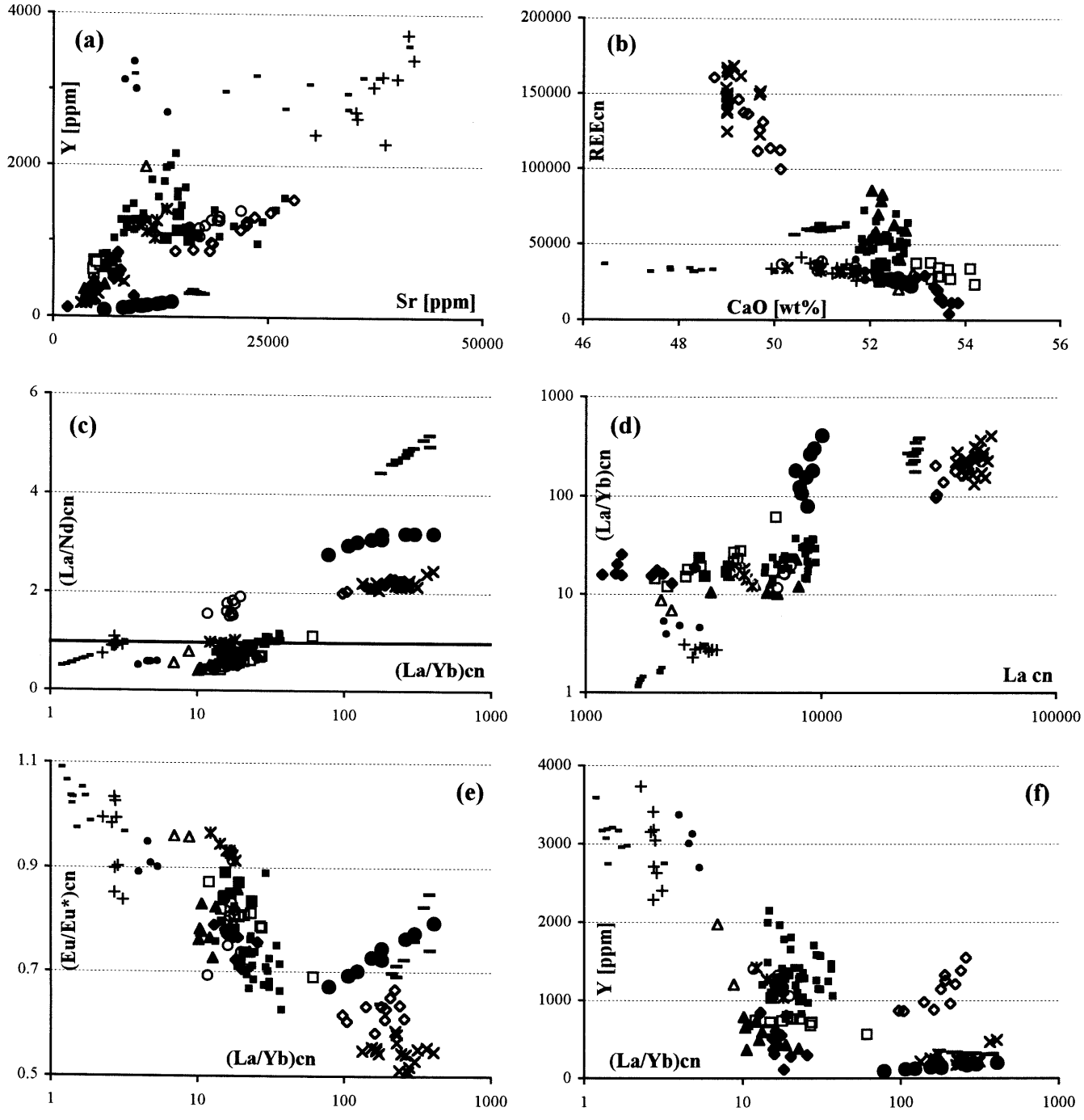

Fig. 5 Trace element characteristics of fluorapatites compiled from Fig. 3 including samples N602 (*long dashes*) and OK8 (*large dots*). *Other symbols* as in Fig. 3

Sr concentration with R = 0.5 for all analyses performed. Except for sample HC559, a negative linear correlation is observed between the CaO content and ΣREE (Fig. 5b), suggesting that the REE predominantly replace Ca in the fluorapatite structure (Hughes et al. 1991). The fluorapatites of the Homa samples display overall high Na_2O values up to 4 wt%, which decrease as ΣREE and $(La/Yb)_{cn}$ increase (Table 4). All other samples have Na_2O well below 1 wt% with no systematic variation.

Discussion

Relationships between carbonatite fractionation and fluorapatite REE composition

We observe the same relationships in the fluorapatite REE patterns for the entire data set as for the individual carbonatite complexes. There is a positive correlation

between the ratios $(La/Yb)_{cn}$ and $(La/Nd)_{cn}$ (Fig. 5c). Fluorapatites with a convex-upward shaped REE pattern tend to have an overall flat REE slope. As $(La/Nd)_{cn}$ ratios increase from <1 to >1, the patterns successively steepen to increasing $(La/Yb)_{cn}$ ratios. This relationship also holds for individual analyses of the particular samples (Fig. 3). The La_{cn} content is clearly correlated with the shape of the REE pattern expressed as $(La/Yb)_{cn}$ with $R = 0.79$ (Fig. 5d). Thus, fluorapatites with a high La content (and therefore a high ΣREE content) have a steep REE pattern, a high $(La/Yb)_{cn}$ ratio, and a straight distribution on a chondrite-normalized REE plot. The same relationships were observed in the literature data set of fluorapatite compositions (Fig. 1). The key question is, whether the relationship between the ΣREE content and the shape of the REE pattern is a function of carbonatite magma evolution.

To investigate this issue, it is necessary to interpret the samples in terms of their degree of differentiation. For Otjisazu, field relationships as outlined previously indicate a fractionation sequence from clinopyroxenites (with early calciocarbonatite bodies) through flow-banded pyroxene–calcite rocks to the central calciocarbonatites with interspersed wollastonite-rich lenses at their base. Within this sequence, the La contents of fluorapatites increase, as do the ratios $(La/Nd)_{cn}$ and $(La/Yb)_{cn}$ (Fig. 3). For the Homa Mountain bulk samples, the CaO contents decrease from HC559 to HC554 to HC34 with a concomitant increase in Fe_2O_3(tot) and MgO, an evolution generally considered to reflect a differentiation sequence controlled by the crystallization of calcite (e.g., Le Bas 1989; Wyllie 1989; among many others). In line with the relationships derived from Otjisazu, the La content of Homa fluorapatite increases in this fractionation sequence from HC559 (La = 450 ppm) to HC554 (741 ppm) to HC34 (1,637 ppm) (Table 4, Fig. 3). At the same time, the ratio $(La/Nd)_{cn}$ increases from 0.6 to 1.7, and $(La/Yb)_{cn}$ increases from 1.6 to 2.7 to 16.7, suggesting that the Homa samples also represent a similar fractionation suite.

The Kalkfeld and Ondurakorume whole rock samples are poor in MgO. Considering the occurrence of late magnesiocarbonatites at Ondurakorume, the calciocarbonatites analyzed here should represent early carbonatites within these complexes. From the relationships discerned above, their fluorapatites should have low $(La/Nd)_{cn}$ and $(La/Yb)_{cn}$ ratios and overall moderate REE contents. Indeed, all four fluorapatite samples from these intrusions have convex-upward shaped REE patterns and moderate $(La/Yb)_{cn}$ ratios between 4.7 and 18.0 (Table 2). Also, they have only moderate La_{cn} contents in comparison to many other fluorapatites (Fig. 3). A differentiation sequence for the samples can be established neither from field relationships nor from whole rock composition. However, there is again a positive correlation between $(La/Yb)_{cn}$ and $(La/Nd)_{cn}$, and between the La content and the steepness of the REE patterns expressed as the ratio $(La/Yb)_{cn}$ for the Kalkfeld suite (Fig. 3). As expected from the high La contents of 5,800 ppm in N602 fluorapatites, they also display a straight REE distribution with high $(La/Nd)_{cn}$ and $(La/Yb)_{cn}$ ratios (Fig. 5). The same applies to OK8 fluorapatites. Significantly, these fluorapatites which crystallized from a carbonatitic fluid by reaction with a country rock, plot slightly displaced from the general trend in Fig. 5d, e.

From these relationships we suggest that early fluorapatite within a given sequence of carbonatite differentiation has the lowest La and REE contents, and convex-upward shaped REE patterns with $(La/Nd)_{cn}$ ratios <1 and low $(La/Yb)_{cn}$ values. The patterns are slightly different in the various carbonatite complexes with respect to the peak of the convex-upward shape. With differentiation of the carbonatite magma, the fluorapatites increasingly incorporate La and ΣREE. This relationship was previously noted by Le Bas and Handley (1979), who observed higher La and Ce concentrations in fluorapatites from alvikites than in fluorapatites from sövites that are parental to the alvikites, and by Zaitsev and Bell (1995) studying fluorapatite compositions in early and late carbonatites and phoscorites from the Kovdor carbonatite. Knudsen (1991) also reported an increase of ΣREE and a concomitant increase of the ratio LREE/HREE in fluorapatites from early to late carbonatites in Greenland, and noted that this evolution may even apply to the core towards rim compositions of individual fluorapatite crystals. The

Table 5 Distribution coefficients and parental melt compositions (PMC). Distribution coefficients *Fug* Fugimaki (1986), *F and P* Fleet and Pan (1997), *Nag* Nagasawa (1970), *TS 1* suggested D values fluorapatite/carbonatite melt, *TS2* modified TS1 values at overall higher values, *TS3* calcite/carbonatite D values applied, *Klem* D values clinopyroxene/carbonatite melt (Klemme et al. 1995). *PMC* Parental Melt Composition (in ppm) extending over 2.5, 3.0, and 2.0 orders of magnitude

		La	Ce	Pr	Nd	Sm	Eu	Gd	Tb	Dy	Ho	Er	Tm	Yb	Lu
Apatite	Fug	14.5	21.1		32.8	46	25.5	43.9	–	34.8	–	22.7	–	15.4	13.8
F-apatite	F and P	5.3	7.3	8.2	8.4	7.8	6.7	5.7	–	3.9	–	2.5	–	1.4	–
Apatite	Nag		29.6	–	57.1	84.8	9.22	–	–	246	–	275	–	232	199
F-apatite	TS1	0.9	1.8	2.4	2.8	3.6	4.1	4.5	4.8	5.1	5.4	5.6	5.8	6.0	6.2
F-apatite	TS2	1.5	2.5	3.4	4.5	6.5	7.1	7.5	7.8	8.1	8.4	8.7	9.1	9.5	10.0
Calcite	TS3	0.05	0.045	0.04	0.035	0.029	0.026	0.023	0.02	0.018	0.016	0.014	0.013	0.011	0.01
Cpx	Klem	0.07	0.09	0.11	0.11	0.13	0.22	0.26	–	0.29	–	0.41	–	–	–
PMC	2.5	1,000	2,100	255	1,020	220	67	190	29	150	27	64	8	43	5
PMC	3.0	1,000	1,775	177	665	122	33	82	11	51	8.5	17	1.9	9	1
PMC	2.0	500	1,070	135	570	135	42	125	20	115	22	53	7	40	5

present data suggests that, with increasing La and ΣREE content of the fluorapatites, early convex-upward shaped REE patterns are leveled out, and the ratios $(La/Nd)_{cn}$ and $(La/Yb)_{cn}$ increase. The positive correlation between La (or ΣREE) and $(La/Yb)_{cn}$ is independent of the whole rock composition. Sample OS69 contains high-La fluorapatite with a high $(La/Yb)_{cn}$ ratio, although the Si-rich bulk rock is low in ΣREE (Table 1), because that fluorapatite crystallized late in the Otjisazu fractionation sequence. Conversely, the Kalkfeld and Ondurakorume carbonatites represent REE-rich carbonatite magma systems with high ΣREE in the whole rocks (Table 1), but contain fluorapatite with a low La content and low $(La/Yb)_{cn}$ which crystallized early in the respective carbonatite bodies. Also, fluorapatite in early calciocarbonatites at Otjisazu (OS155) are distinctly different in REE composition from the fluorapatite in late calciocarbonatites (OS95).

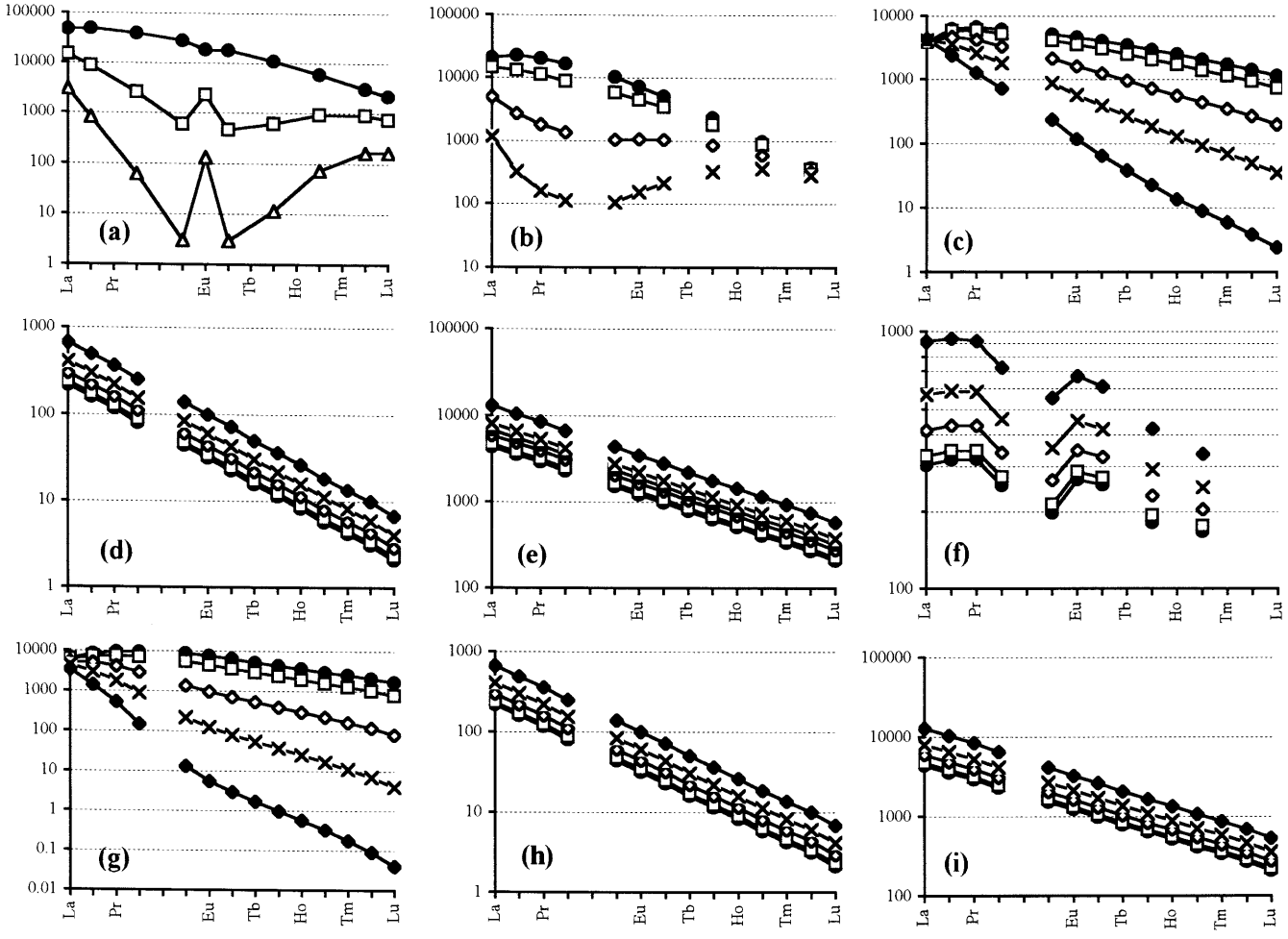

Fig. 6 Model calculations (Rayleigh fractionation) for the evolution of minerals and melts in a carbonatitic magma. Closed system conditions along the liquid lines of descent. See Table 5 for distribution coefficients and parental melt composition (PMC 2.5). All values chondrite-normalized after Anders and Grevesse (1989). **a** Apatite REE patterns applying the apatite/dacitic melt partition coefficients of Fugimaki (1986). Fractionation increments f = 0.98 (*dots*), 0.9, and 0.8 (*open triangles*). Note the depletion in MREE. Table 6 runs 3–4. **b** Calculated fluorapatite composition with distribution coefficients fluorapatite/phosphate–fluoride melt (Fleet and Pan 1997). Fractionation increments f = 0.98 (*dots*), 0.9, 0.7, and 0.5 (*crosses*). Table 6 runs 5–7. **c**, **d**, **e** Calculated REE patterns for fluorapatite **c**, calcite **d**, and residual melt **e** applying the suggested distribution coefficient set TS1. Fractionation increments f = 0.98 (*dots*), 0.9, 0.7, 0.5, and 0.3 (*full diamonds*). Table 6 runs 8–11. **f** Calculated clinopyroxene composition applying the clinopyroxene/carbonatite melt distribution coefficients of Klemme et al. (1995). Fractionation increments f = 0.98 (*dots*), 0.9, 0.7, 0.5, and 0.3 (*full diamonds*). Table 6 runs 15–16. **g**, **h**, **i** Calculated composition of fluorapatite **g**, calcite **h**, and residual melt **i**. Distribution coefficient set fluorapatite/carbonatite melt TS2 with overall higher values especially for the MREE. Note the flat REE pattern of fluorapatite at low degree of fractionation. Fractionation increments f = 0.98 (*dots*), 0.9, 0.7, 0.5, and 0.3 (*full diamonds*). Table 6 runs 17–20

Derivation of partition coefficients for fluorapatite in carbonatite magmas

The data suggest a relationship between the fluorapatite REE concentrations and the shape of the REE patterns, and the differentiation of the parental carbonatite magma. To investigate this issue, we conducted model calculations with a Rayleigh fractionation model for the REE depending on the parameters: distribution coefficient fluorapatite/carbonatite melt $D^{REE}_{fluorapatite/melt,}$ pa-

Table 6 Model calculations for fluorapatite, calcite, and clinopyroxene REE compositions in carbonatite melt. *Column 1*: *PMC* Parental Melt Composition. 2.5 and 3.0 orders of magnitude from La (1,000 ppm) to Lu (5 ppm), and from La (1,000 ppm) to Lu (1 ppm), respectively, see Table 5. *Column 2*: Mode of fractionation *LLD* liquid lines of descent (closed system Rayleigh fractionation), *SM* sequential mode, in which each residual melt increment is treated parental to the successive crystallization increment. *Column 3*: D-Ap distribution coefficient applied, *Fug* apatite in dacite melt (Fugimaki 1986), *F and P* fluorapatite in synthetic phosphate–fluoride melt (Fleet and Pan 1997), *TS1* this study, suggested D values fluorapatite/carbonatite melt, *TS2* overall slightly higher D values than TS1. See Table 5 for absolute values. *Columns 4–6*: Proportions of crystallizing fluorapatite (*Fap*), calcite (*Cc*), and clinopyroxene (*Cpx*). *Column 7*: *f* degree of fractionation (fraction of melt remaining). *Columns 8–18*: Chondrite-normalized REE characteristics of the residual liquids (8–10), and crystallizing fluorapatite (11–13), calcite (14–16), and clinopyroxene (17–18)

Run	1 PMC	2 Mode	3 D-Ap	4 Fap	5 Cc	6 Cpx	7 f	8 La/Yb Liqu.	9 La/Nd Liqu.	10 La Liqu.	11 La/Yb Fap	12 La/Nd Fap	13 La Fap	14 La/Yb Cc	15 La/Nd Cc	16 La Cc	17 La/Nd Cpx	18 La Cpx
1	2.5	–	–	–	–	–	1.0	16.1	1.89	4,260	–	–	–	–	–	–	–	–
2	3.0	–	–	–	–	–	1.0	76.9	2.89	4,260	–	–	–	–	–	–	–	–
3	2.5	LLD	Fug	0.02	0.98	–	0.98	16.1	1.90	4,318	15.4	1.21	47,033	70.0	2.7	217	–	–
4	2.5	LLD	Fug	0.02	0.98	–	0.80	16.0	2.04	4,938	18.5	49.6	3,037	69.4	2.7	263	–	–
5	2.5	LLD	F and P	0.02	0.98	–	0.98	16.1	1.89	4,334	56.3	1.27	20,703	70.0	2.7	217	–	–
6	2.5	LLD	F and P	0.02	0.98	–	0.80	15.7	1.91	5,145	25.5	2.38	8,650	69.4	2.7	263	–	–
7	2.5	LLD	F and P	0.02	0.98	–	0.50	14.9	1.95	7,653	4.1	10.2	1,146	68.2	2.7	411	–	–
8	2.5	LLD	TS1	0.02	0.98	–	0.98	16.1	1.89	4,342	3.0	0.68	3,842	70.0	2.7	217	–	–
9	2.5	LLD	TS1	0.02	0.98	–	0.9	16.2	1.89	4,701	4.4	0.78	3,875	69.7	2.7	235	–	–
10	2.5	LLD	TS1	0.02	0.98	–	0.6	16.5	1.91	6,862	25.1	1.56	4,035	68.6	2.7	346	–	–
11	2.5	LLD	TS1	0.02	0.98	–	0.3	17.1	1.93	13,102	494	5.1	4,325	66.8	2.7	668	–	–
12	2.5	LLD	TS1	0.1	0.9	–	0.9	16.8	1.92	4,667	4.4	0.78	3,875	69.7	2.7	235	–	–
13	2.5	LLD	TS1	0.1	0.9	–	0.6	19.7	2.05	6,628	25.1	1.56	4,035	68.6	2.7	346	–	–
14	2.5	LLD	TS1	0.1	0.9	–	0.3	25.9	2.28	12,072	494	5.1	4,325	66.8	2.7	668	–	–
15	2.5	LLD	TS1	0.1	0.5	0.4	0.8	17.5	1.97	5,159	7.3	0.96	3,921	69.4	2.7	263	1.21	367
16	2.5	LLD	TS1	0.1	0.5	0.4	0.5	21.0	2.14	7,717	54.9	2.13	4,110	68.2	2.7	411	1.24	568
17	2.5	LLD	TS2	0.02	0.98	–	0.98	16.1	1.89	4,341	2.9	0.67	6,327	70.0	2.7	217	–	–
18	2.5	LLD	TS2	0.02	0.98	–	0.9	16.3	1.90	4,695	5.9	0.86	6,063	69.7	2.7	235	–	–
19	2.5	LLD	TS2	0.02	0.98	–	0.6	17.1	1.93	6,820	151	2.92	4,951	68.4	2.7	346	–	–
20	2.5	LLD	TS2	0.02	0.98	–	0.3	18.7	2.00	12,914	38,750	23.3	3,501	66.8	2.7	668	–	–
21	2.5	SM	TS1	0.02	0.98	–	0.98	16.1	1.89	4,342	2.68	0.63	3,842	69.9	2.7	217	–	–
22	2.5	SM	TS1	0.02	0.98	–	0.9	16.2	1.89	4,790	4.14	0.74	3,949	69.8	2.7	240	–	–
23	2.5	SM	TS1	0.02	0.98	–	0.6	16.8	1.93	8,228	34.2	1.63	7,793	71.8	2.7	668	–	–
24	2.5	SM	TS1	0.02	0.98	–	0.3	19.3	2.02	59,488	1,344	6.4	60,389	80.2	2.8	9,335	–	–
25	2.5	SM	TS1	0.1	0.9	–	0.9	16.8	1.92	4,667	4.4	0.78	3,875	69.7	2.7	235	–	–
26	2.5	SM	TS1	0.1	0.9	–	0.7	19.3	2.03	6,354	13.5	1.22	4,353	72.0	2.7	327	–	–
27	2.5	SM	TS1	0.1	0.9	–	0.5	25.4	2.26	11,573	65.9	2.28	6,129	81.8	2.9	614	–	–
28	3.0	SM	TS1	0.02	0.98	–	0.98	77.0	2.90	4,342	14.5	1.04	3,842	334	4.1	217	–	–
29	3.0	SM	TS1	0.02	0.98	–	0.7	78.3	2.92	6,056	61.8	1.84	4,049	330	4.1	305	–	–
30	3.0	SM	TS1	0.02	0.98	–	0.5	81.0	2.95	11,563	267	3.28	5,841	332	4.1	585	–	–
31	3.0	SM	TS1	0.1	0.5	0.4	0.8	85.3	3.03	7,332	35.4	1.47	5,573	338	4.2	374	1.87	521
32	3.0	SM	TS1	0.1	0.5	0.4	0.5	111	3.43	13,281	291	3.41	7,973	361	4.3	708	1.98	978

rental melt composition L_0, degree of fractionation f (fraction of melt remaining), and fractionating mineral assemblage. The parental melt composition L_0 was chosen to extend over 2.5 and 3 orders of magnitude from La to Lu (Table 5), which is characteristic for many carbonatites (Möller et al. 1980; Nelson et al. 1988; Woolley and Kempe 1989; Keller and Spettel 1995; Hornig-Kjarsgaard 1998; Bühn and Rankin 1999). The fractionating minerals considered are fluorapatite and calcite, commonly dominant liquidus phases in carbonatite magmas (Biggar 1969; Wyllie 1989; Barker 1993; Morogan and Lindblom 1995), and also clinopyroxene to account for the Otjisazu system and other Si-bearing carbonatite magmas (e.g., Phalaborwa, Eriksson et al. 1985; Eriksson 1989). Partition coefficients for clinopyroxene/carbonatite melt were taken from Klemme et al. (1995) determined at 20–22 kbar and 1,050–1,100 °C (Table 5). Calcite contains generally much less REE than carbonatite whole rocks (e.g., Hornig-Kjarsgaard 1998), which suggests REE distribution coefficients for calcite significantly <1. Calcite has a preference for LREE over MREE and HREE in the mineral/fluid system (Zhong and Mucci 1995; Rimstidt et al. 1998) but quantitative coefficients for calcite/carbonatite melt have not yet been determined. Preliminary results obtained by K.M. Law (personal communication) suggest a slope from La to Lu of half a magnitude at most. Distribution coefficients were therefore chosen here to extend from 0.05 for La to 0.01 for Lu (Table 5). To our knowledge, distribution coefficients for the system fluorapatite/carbonatite melt are unknown so far.

To test established partition coefficients apatite/melt, calculations were performed for the systems apatite/silicate melt (e.g., Nagasawa 1970; Paster et al. 1974; Watson and Green 1981; Fugimaki 1986), and for fluorapatite in a synthetic phosphate–fluoride melt (Fleet and Pan 1997, Table 5). Applying the Fugimaki (1986) data set for dacitic silicate melts, crystallizing fluorapatite would be heavily depleted in MREE with a convex-downward REE pattern even at low degrees of fractionation $f=0.9$ (Fig. 6a). This trend evolves at $f=0.80$ towards $(La/Nd)_{cn}$ values even higher than $(La/Yb)_{cn}$ values (49.6 and 18.5, respectively, Table 6 runs 3–4), which reflects an extremely depleted MREE pattern at a low La_{cn} content. For the synthetic system fluorapatite/phosphate–fluoride melt, even relatively low degrees of fractionation ($f=0.8$) yield a convex-downward shaped REE pattern for fluorapatites which is further accentuated at $f=0.5$ (Fig. 6b). The La content in fluorapatites drastically decreases with differentiation but the Yb remains constant, resulting in decreasing $(La/Yb)_{cn}$ ratios during differentiation (Table 6 runs 5–7). No $(La/Nd)_{cn}$ values <1 are observed. Assuming equilibrium crystallization, the La concentration in fluorapatite increases slightly with f, and the downward shaped patterns are slightly suppressed (not shown). However, the ratio $(La/Nd)_{cn}$ is still >1 for all increments, and $(La/Yb)_{cn}$ values again decrease with increasing differentiation. Hence, distribution coefficients for apatite in silicate and synthetic phosphate–fluoride melt systems are not able to produce the observed composition of carbonatitic fluorapatites.

To account for the observed REE trends in natural fluorapatites, a data set for $D^{REE}_{fluorapatite/carbonatite\ melt}$ was constructed that has a positive slope from La to Lu throughout. The absolute D values (TS1, Table 5) were chosen between those published for the silicate melt system (e.g., Fugimaki 1986), and for the synthetic phosphate–fluoride melt system (Fleet and Pan 1997). Fractionation increments from $f=1.0$ to $f=0.3$ were calculated at various modal proportions fluorapatite/calcite/clinopyroxene. At a ratio fluorapatite/calcite $=0.02/0.98$, fluorapatite reproduces the spread of $(La/Nd)_{cn}$ and $(La/Yb)_{cn}$ ratio as for the natural fluorapatites at moderately increasing La contents (Fig. 6c, Table 6 runs 8–11). Crystallizing calcite would have a straight REE pattern (Fig. 6d), similar to calcite analyses from worldwide carbonatites (e.g., Hornig-Kjarsgaard 1998). The residual melts preserve their straight REE patterns at increasing La and ΣREE contents (Fig. 6e) and constant $(La/Yb)_{cn}$ ratios between 16 and 17. Modifying the modal ratio fluorapatite/calcite to 0.1/0.9 yields the same REE patterns for fluorapatite and calcite, but the residual melts display a more prominent steepening of their REE patterns as expressed by an increase of the ratio $(La/Yb)_{cn}$ from 16.1 ($f=1.0$) to 25.9 ($f=0.3$) (Table 6 runs 12–14). The amount of clinopyroxene crystallization has no significant effect. Crystallization of fluorapatite, calcite, and clinopyroxene at proportions 0.1/0.5/0.4 yields a slightly LREE-enriched clinopyroxene REE pattern (Fig. 6f) and a more pronounced increase of residual melt $(La/Yb)_{cn}$ ratios with increasing f (Table 6 runs 15–16) comparable to runs 12–14 in Table 6 without clinopyroxene fractionation.

It is known that distribution coefficients are affected by the bond valence and the effective size of the two structural Ca^{2+} sites in fluorapatite occupied by the REE (Hughes et al. 1991; Fleet and Pan 1995b), and by the melt polymerization and the activity of the REE-complexing components OH, F, Cl, and CO_2 species in the melt (Watson and Green 1981; Cantrell and Byrne 1987; Ellison and Hess 1989; Wood 1990). It can be seen that slight variations in the TS1 values for the MREE will determine the peak location of convex-upward shaped REE patterns. This may be the reason for the different peak positions in convex-upward fluorapatite patterns in the individual carbonatite complexes. For example, when the D values for the MREE are increased at overall higher D values for the entire group of the REE (from La = 1.5 to Lu = 10.0, TS2 in Table 5), the REE patterns of fluorapatite are flatter at low degrees of fractionation and therefore have peaks shifted towards the MREE (Fig. 6g). At high degrees of fractionation, fluorapatites will then have exceedingly high values of $(La/Yb)_{cn}=38{,}750$ at $f=0.3$ (Table 6 runs 17–20). Apart from the absolute D values, the parental melt composition affects the REE characteristics of crystallizing fluorapatite. The suggested $D^{REE}_{fluorapatite/carbonatite\ melt}$

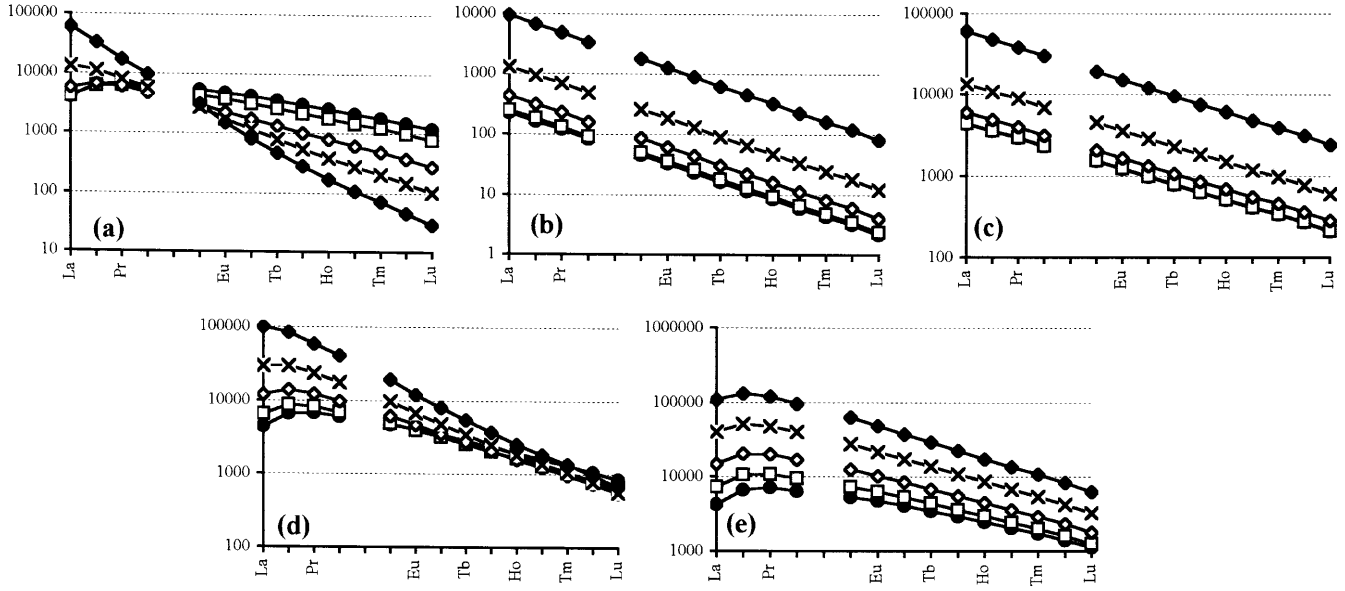

Fig. 7 Model calculations applying episodic, sequential crystallization of fluorapatite. **a** Fluorapatite. **b** Calcite. **c** Residual melt. Sequential mode 10%. Fractionation increments f = 0.98 (*dots*), 0.9, 0.7, 0.5, and 0.3 (*full diamonds*). Table 6 runs 21–24. **d** Fluorapatite composition, same parameters as in **a**, but 5% sequential mode. Fractionation increments f = 0.9 (*dots*), 0.8, 0.7, 0.6, and 0.5 (*full diamonds*). **e** Fluorapatite composition as in **d**, but 1% sequential mode. Fractionation increments f = 0.95 (*dots*), 0.9, 0.85, 0.8, and 0.75 (*full diamonds*)

set (TS1 in Table 5) is therefore not considered to represent absolute values in a strict sense for every carbonatite system. However, the important point is that the qualitative shape of D^{REE} for fluorapatite requires D values that increase from La to Lu throughout to account for the observations made in the natural samples. It is interesting to note that a qualitatively comparable $D^{REE}_{apatite/melt}$ pattern at overall higher D values was reported for apatite in a granitic system (Nagasawa 1970, Table 5) which, however, is "for the most part ignored by modelers" (Watson and Green 1981). Only one fluorapatite REE pattern with a positive slope from La to Lu was found in the literature. This fluorapatite derives from a magnetite–fluorapatite ore in India with a supposed granitic/hydrothermal origin (Frietsch and Perdahl 1995), and, significantly, a low ΣREE content. Such patterns can develop in a parental melt with a flat REE pattern only. The highly LREE-enriched character of carbonatite systems will dominate over the effect of the partition coefficients, so that such fluorapatite REE patterns will not develop in carbonatite magmas.

Modes of fluorapatite crystallization

Although the proposed D values for fluorapatite/carbonatite melt reproduces the observed evolution of $(La/Nd)_{cn}$ and $(La/Yb)_{cn}$ values, the La and ΣREE evolution in individual carbonatite complexes cannot be achieved with the parameters applied. For instance, La_{cn} increases from 2,194 to 4,686 in the Kalkfeld/Ondurakorume fluorapatites, from 1,917 to 6,975 at Homa, and from 1,670 to 45,325 at Otjisazu, but in the calculations the La_{cn} content increases only moderately from 3,842 (f = 0.98) to 4,325 at f = 0.3 (Table 6 runs 8–11). There is no set of distribution coefficients that could meet the observed positive correlation between $(La/Nd)_{cn}$, $(La/Yb)_{cn}$, and La_{cn}. Moreover, neither equilibrium nor in situ crystallization processes (Langmuir 1989) could produce greater La contents than those calculated with a Rayleigh fractionation model. One option to increase the La content of fluorapatites within a given fractionation sequence is to treat the crystallization increments as individual melt systems, hence taking each residual melt composition as the parental melt for the successive fractionation increment (sequential mode in Table 6). The petrological meaning of this treatment is that crystallization of the (near)-liquidus phases, fluorapatite and calcite, drives the melt towards a composition that is no longer saturated in these phases, especially in fluorapatite. At further cooling, the evolved melt will only precipitate fluorapatite when phosphate saturation is achieved again. Consequently, the melt behaves as an independent melt system at each step of the sequential fluorapatite precipitation, and does not follow liquid lines of descent in a closed system. This process is seen in nature in the form of well-defined fluorapatite layers and stringers in carbonatite bodies during all stages of carbonatite evolution.

Results for the episodic fluorapatite crystallization mode show that La_{cn} and ΣREE in fluorapatite increases with fractionation, depending on the steps of episodic fluorapatite precipitation. Sequential increments of f = 0.1 mimic episodes of instantaneous fluorapatite crystallization as saturation is reached every 10% of bulk melt crystallization. La_{cn} in fluorapatite increases from 3,842 to 60,389 as fractionation proceeds from f = 0.98 to f = 0.3 (Fig. 7a, Table 6 runs 21–24), and

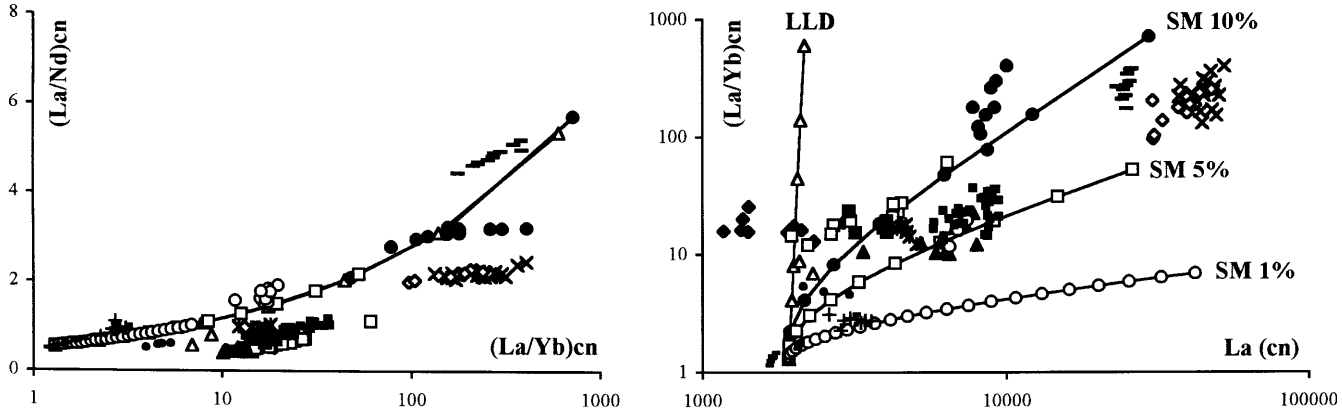

Fig. 8 Comparison between observed fluorapatite compositions and model calculations. The calculations use a PMC composition extending from La = 500 ppm over two orders of magnitude (PMC 2.0, Table 5) to meet the evolution of the entire data set. *Connected triangles* closed system conditions, LLD mode, f = 1.0–0.3. *Connected dots* sequential mode 10%, f = 1.0–0.3. *Connected open squares* 5% sequential mode, f = 1.0–0.5. *Connected open circles* 1% sequential mode, f = 1.0–0.75. Sample symbols as in Figs. 3 and 5. See text for explanations

therefore covers the spread of fluorapatite La concentrations from the literature data set (Fig. 1) and those studied here. La_{cn} in calcite increases from 217 to 9,335. The calculated calcite compositions (Fig. 7b) compare well with the calcite analyses from carbonatites which have straight REE patterns extending over two to three orders of magnitude with $(La/Yb)_{cn} = 54–504$ and $La_{cn} = 490–1{,}660$ noted by Hornig-Kjarsgaard (1998). The ΣREE concentrations and $(La/Yb)_{cn}$ ratios of the residual melts (Fig. 7c) depend on the volumetric proportions of fluorapatite and calcite. The more fluorapatite crystallizes (Table 6 runs 25–27), the greater the steepness of the REE pattern of the residual melts with $(La/Yb)_{cn} = 25.4$ at f = 0.5, as sometimes observed in cogenetic sequences of natural carbonatites (e.g., Woolley and Kempe 1989; Knudsen 1991). At an REE composition of L_0 extending over three orders of magnitude, the fluorapatites evolve from $(La/Yb)_{cn} = 14.5$ to 267 and $La_{cn} = 3{,}842$ to 5,841 at f = 0.98–0.5, and the residual melts from $(La/Yb)_{cn} = 77.0$ to 81.0 at $La_{cn} = 4{,}342$ to 11,563 (Table 6 runs 28–30). Again, clinopyroxene fractionation has an only minor effect on the REE composition of the residual carbonatite magmas (Table 6 runs 31–32).

The more often phosphate saturation is reached, the more fluorapatite is enriched in La and ΣREE through melt evolution. Sequential increments of f = 0.05 (5% mode) yield an even more pronounced La_{cn} and ΣREE enrichment in fluorapatites at increasing $(La/Nd)_{cn}$ and $(La/Yb)_{cn}$ with fractionation from 0.95 to 0.50 (Fig. 7d). As the increments are further increased to f = 0.01 steps (1% mode), the La_{cn} and ΣREE values increase enormously at only moderate $(La/Yb)_{cn}$ and $(La/Nd)_{cn}$ ratios (Fig. 7e). While, for example, the 10% sequential mode, represents fluorapatite saturation every 10% of whole melt crystallization (and instantaneous precipitation of fluorapatite in layers, pods, or stringers as observed at Homa), closed system conditions represent fluorapatite crystallization following a liquid line of descent, yielding disseminated fluorapatite as also observed in many carbonatites. The ratio of closed system conditions versus episodic crystallization of fluorapatite will determine the amount of ΣREE enrichment in fluorapatites, while their $(La/Nd)_{cn}$ and $(La/Yb)_{cn}$ ratios are not affected by the mode of fractionation (Fig. 8a). This ratio may vary between individual carbonatite systems, depending on the predominance of closed system conditions or episodic fluorapatite crystallization. All modes of crystallization yield virtually the same correlation between $(La/Yb)_{cn}$ and $(La/Nd)_{cn}$ and compare with the entire fluorapatite data set (Fig. 8a), but reach a given $(La/Yb)_{cn}$ and $(La/Nd)_{cn}$ ratio at different degrees of fractionation. The slope of La enrichment in fluorapatites, however, differs between the different modes (Fig. 8b). For the entire data set, the trend of fluorapatite composition suggests episodic fluorapatite crystallization about every 5–10% of whole melt fractionation.

Implications from redox-sensitive REE and Y

A negative $(Ce/Ce^*)_{cn}$ anomaly is observed only in early fluorapatites. Accordingly, apatites from the Jacupiranga and Phalaborwa carbonatites (Hornig-Kjarsgaard 1998), which display a convex-upward shaped LREE pattern, and therefore indicate crystallization during early carbonatite fractionation, have a very slight negative Ce anomaly developed. However, a control via Ce-rich trace minerals (e.g., pyrochlore) cannot be excluded. A more systematic behavior is observed with respect to a $(Eu/Eu^*)_{cn}$ anomaly which tends to develop from early to late fluorapatites with increasing $(La/Yb)_{cn}$. This is manifested within individual carbonatite complexes (Fig. 3), and in the entire data set (Fig. 5e). Significant negative Eu anomalies in fluorapatite are therefore encountered only in evolved carbonatites. Although rarely observed in carbonatite whole rocks or minerals, negative Eu anomalies were reported from calcite and a whole rock analysis of a late-stage sövite at Phalaborwa (Hornig-Kjarsgaard 1998). The negative correlation between $(La/Yb)_{cn}$ and $(Eu/Eu^*)_{cn}$ is reversed into a

positive correlation in sample OK8 (Fig. 5e), stressing the non-magmatic nature of these fluorapatites.

Although Kapustin (1980) reported pyrrhotite in both early and late carbonatites suggesting that low fO_2 conditions may prevail throughout carbonatite differentiation, most other indications point to an increasing oxygen fugacity during fractionation of carbonatite magmas. Pyrrhotite occurs trapped in fluid inclusions in apatites of early sövite in East Africa (Rankin 1975), and has not been observed in later carbonatite, but pyrite has. More usually, the S-bearing mineral in late carbonatites is barite (Kapustin 1980), indicating a high fO_2 level. Moreover, the $\delta^{34}S$ values of carbonatitic sulfides were found to decrease towards late-stage carbonatites suggesting an increase in oxidizing conditions during carbonatite evolution (Deines 1989). After all, there is no generally valid and quantitatively constrained scheme for the evolution of fO_2 in carbonatite magmas, and REE anomalies observed in carbonatitic fluorapatites can hardly be considered to reflect the oxidation state of the parental magma. Fractionation of a Eu^{2+}-accumulating mineral phase is not a viable mechanism to explain the Eu anomalies in the fluorapatites, because neither apatite (e.g., Watson and Green 1981) nor clinopyroxene (Klemme et al. 1995) have a preference for Eu^{2+} relative to trivalent REEs.

A more tempting option is the partitioning of Eu^{2+} into a coexisting aqueous fluid as suggested for granitic systems (Candela 1990). On that basis, Irber (1999) interpreted strongly negative Eu anomalies in highly evolved granitic rocks as being due to preferential partitioning of Eu^{2+} into a coexisting high-temperature fluid. Möller and Dulski (1999) also noted that Eu^{2+} is largely retained in an aqueous solution relative to the trivalent REEs. Many carbonatite complexes show evidence for an exsolution of an H_2O–CO_2 fluid phase expelled as fenitizing fluid (e.g., Bailey 1993; Samson et al. 1995). This also applies to the Kalkfeld complex (Bühn and Rankin 1999), and to the Homa carbonatite (Le Bas 1977). The minor fenitization aureole at Otjisazu is attributed to the deep level of erosion there (Bühn et al. 2001). The appreciable solubility of 9.76 ± 0.68 wt% H_2O in carbonatite melt at 1 kbar and 900 °C (H. Keppler, personal communication 2000) is experimental evidence for the potential of carbonatite magmas to dissolve water, which can later be exsolved during cooling and crystallization. Likewise, it may therefore be envisaged for carbonatite systems, that Eu^{2+} is continuously extracted from carbonatite magmas via an aqueous fluid. Support for this interpretation comes from the fact that the highest Y concentrations are observed in early fluorapatites (Fig. 5f), because Y will also tend to be retained in solution together with Eu^{2+} (Möller and Dulski 1999). The highest Y/Ho ratios, distinctly above the chondritic ratio of 28, are therefore observed in early, REE-poor fluorapatites (Tables 2, 3, 4). The amount of Y depletion in the melt, however, will depend on the dominant complexing agents in the system, because Y may behave differently in fluorine- and carbonate-dominated fluid systems, respectively (Bau and Dulski 1995). Both the fO_2 of the carbonatite system, and the dominant complexing mechanism in the coexisting fluid, may vary between individual carbonatite systems.

Conclusions

The REE composition of carbonatitic fluorapatites can be related to different stages of carbonatite differentiation. Early fluorapatites tend to have low REE contents hardly above 1,500 ppm La in the sample suite investigated, regardless of the REE content of the whole rock. Their $(La/Yb)_{cn}$ ratios are generally below 100, and they have $(La/Nd)_{cn}$ ratios close to or below unity. Where this ratio is < 1, the convex-upward shape of their REE pattern peaks between Pr and Eu. High fluorapatite REE contents up to 1 wt% La in the samples investigated point to crystallization from an evolved carbonatite melt. Such fluorapatites have $(La/Nd)_{cn} > 1$ and a straight REE pattern extending over two orders of magnitude or more from La to Yb. Their $(La/Yb)_{cn}$ ratios are generally above 100.

The $D^{REE}_{fluorapatite/carbonatite\ melt}$ values which can reproduce the observed relationships have a positive slope throughout from La to Lu, with the steepest increase between La and Nd. These largely qualitative D values yield fluorapatite with REE patterns that develop from a convex-upward shape with $(La/Nd)_{cn} \leq 1$ to straight REE patterns with $(La/Nd)_{cn} > 1$ and high $(La/Yb)_{cn}$ ratios as fractionation of the parental carbonatite magma increases. Hence, the REE characteristics of carbonatitic fluorapatites – often in contrast to the whole rock composition – bear the potential to derive the relative degree of fractionation of individual fluorapatite-bearing carbonatite samples. The modal proportions of fractionating fluorapatite + calcite ± clinopyroxene will determine the slope of the REE patterns of the residual carbonatite melts. Episodic phosphate saturation and crystallization, as manifested in fluorapatite layers throughout carbonatite evolution, may be considered an effective mechanism to increase the La and REE content in fluorapatites which cannot be achieved under closed system conditions.

A $(Eu/Eu^*)_{cn}$ ratio close to unity appears to be indicative of early fluorapatites, while late fluorapatites have a negative $(Eu/Eu^*)_{cn}$ anomaly reaching 0.5 which, however, is not observed in the whole rocks. It is envisaged that an aqueous fluid coexisting with the carbonatite magma from early fractionation on may be able to continuously extract Eu^{2+} from the carbonatite magma. The wide range of Y/Ho ratios, of which the highest values are recorded in early fluorapatites and the lowest values in late fluorapatites, may indicate partitioning of Y into the fluid in a similar manner. However, there is no generally consistent behavior of Y/Ho fractionation. This, and the different location of the peaks of convex-upward shaped REE patterns, suggests that

these parameters depend on the very specific carbonatite melt system with respect to the dominant REE-complexing agents.

Acknowledgements We thank the Hamburg Synchrotron Laboratory (HASYLAB) for access to the facility. We are indebted to Peter Dulski (GFZ Potsdam) who kindly provided the ICP-MS data of the whole rocks. M. Grünhäuser and L. Walz (Giessen) helped with XRF and wet chemical analyses, and Teresa Jeffries (The Natural History Museum, London) is thanked for comparative laser ablation ICP-MS analyses. BB acknowledges financial support by the Deutsche Forschungsgemeinschaft DFG. We also wish to thank Anatoly Zaitsev and an anonymous journal reviewer for constructive comments.

References

Anders E, Grevesse N (1989) Abundances of the elements: meteoritic and solar. Geochim Cosmochim Acta 53:197–214

Ayers JC, Watson EB (1993) Apatite/fluid partitioning of rare-earth elements and strontium: experimental results at 1.0 GPa and 1000 °C and application to models of fluid–rock interaction. Chem Geol 110:299–314

Bailey DK (1993) Carbonate magmas. J Geol Soc Lond 150: 637–651

Barker DS (1993) Diagnostic magmatic features in carbonatites: implications for the origins of dolomite- and ankerite-rich carbonatites. S Afr J Geol 96:131–138

Bau M, Dulski P (1995) Comparative study of yttrium and rare-earth element behaviours in fluorine-rich hydrothermal fluids. Contrib Mineral Petrol 119:213–223

Biggar GM (1969) Phase relationships in the join $Ca(OH)_2$–$CaCO_3$–$Ca_3(PO_4)_2$–H_2O at 1000 bars. Mineral Mag 37:75–82

Binder G, Troll G (1989) Coupled anion substitution in natural carbon-bearing apatites. Contrib Mineral Petrol 101:394–401

Bühn B, Rankin AH (1999) Composition of natural, volatile-rich Na–Ca–REE–Sr carbonatitic fluids trapped in fluid inclusions. Geochim Cosmochim Acta 63:3781–3797

Bühn B, Rankin AH, Radtke M, Haller M, Knöchel A (1999) Burbankite, a (Sr,REE,Na,Ca)-carbonate in fluid inclusions from carbonatite-derived fluids: identification and characterization using Laser Raman, SEM-EDX and synchrotron micro-XRF analysis. Am Mineral 84:1117–1125

Bühn B, Dörr W, Brauns CM (2001) Petrology and age of the Otjisazu carbonatite complex, Namibia: implications for the pre- and synorogenic Damaran evolution. J Afr Earth Sci 32 (in press)

Candela PA (1990) Theoretical constraints on the chemistry of the magmatic aqueous phase. In: Stein HJ, Hannah JL (eds) Ore-bearing granite systems: petrogenesis and mineralizing processes. Geol Soc Am Spec Pap 246, pp 11–20

Cantrell KJ, Byrne RH (1987) Rare earth element complexation by carbonate and oxalate ions. Geochim Cosmochim Acta 51:597–605

Deines P (1989) Stable isotope variations in carbonatites. In: Bell K (ed) Carbonatites: genesis and evolution. Unwin Hyman, London, pp 301–359

Dulski P (1994) Interferences of oxide, hydroxide and chloride analyte species in determination of rare earth elements in geochemical samples by inductively coupled plasma mass spectrometry. Fresenius J Anal Chem 350:194–203

Eby GN (1975) Abundance and distribution of the rare-earth elements and yttrium in the rocks and minerals of the Oka carbonatite complex, Quebec. Geochim Cosmochim Acta 39:597–620

Ellison AJG, Hess PC (1989) Solution properties of rare earth elements: inferences from immiscible liquids. Geochim Cosmochim Acta 53:1965–1974

Emmermann R, Lauterjung J (1990) Double X-ray analysis of cuttings and rock flour: a powerful tool for rapid and reliable determination of borehole lithostratigraphy. Sci Drill 1: 269–282

Eriksson SC (1989) Phalaborwa: a saga of magmatism, metasomatism, and miscibility. In: Bell K (ed) Carbonatites: genesis and evolution. Unwin Hyman, London, pp 221–254

Eriksson SC, Fourie PJ, De Jager DH (1985) A cumulate origin for the minerals in clinopyroxenites of the Phalaborwa Complex. Trans Geol Soc S Afr 88:207–214

Fleet ME, Pan Y (1995a) Crystal chemistry of rare earth elements in fluorapatite and some calc-silicates. Eur J Mineral 7:591–605

Fleet ME, Pan Y (1995b) Site preference of rare earth elements in fluorapatite. Am Mineral 80:329–335

Fleet ME, Pan Y (1997) Rare earth elements in apatite: uptake from H_2O-bearing phosphate–fluoride melts and the role of volatile components. Geochim Cosmochim Acta 61:4745–4760

Fleischer M, Altschuler ZS (1986) The lanthanides and yttrium in minerals of the apatite group – an analysis of the available data. Neues Jahrb Mineral Monatsh 10:467–480

Frietsch R, Perdahl J-A (1995) Rare earth elements in apatite and magnetites in Kiruna-type iron ores and some other iron ore types. Ore Geol Rev 9:489–510

Fugimaki H (1986) Partition coefficients of Hf, Zr and REE between zircon, apatite and liquid. Contrib Mineral Petrol 94:42–45

Gittins J (1989) The origin and evolution of carbonatite magmas. In: Bell K (ed) Carbonatites: genesis and evolution. Unwin Hyman, London, pp 580–600

Hogarth DD (1989) Pyrochlore, apatite and amphibole: distinctive minerals in carbonatite. In: Bell K (ed) Carbonatites: genesis and evolution. Unwin Hyman, London, pp 105–148

Hogarth DD, Hartree R, Loop J, Solberg TN (1985) Rare-earth element minerals in four carbonatites near Gatineau, Quebec. Am Mineral 70:1135–1142

Hornig-Kjarsgaard I (1998) Rare earth elements in sövitic carbonatites and their mineral phases. J Petrol 39:2105–2122

Hughes JM, Cameron M, Mariano AN (1991) Rare-earth-element ordering and structural variations in natural rare-earth-bearing apatites. Am Mineral 76:1165–1173

Irber W (1999) The lanthanide tetrad effect and its correlation with K/Rb, Eu/Eu*, Sr/Eu, Y/Ho, and Zr/Hf of evolving peraluminous granite suites. Geochim Cosmochim Acta 63:489–508

Kapustin YL (1980) Mineralogy of carbonatites. Amerind Publishing Co, New Delhi, India

Keller J, Spettel B (1995) The trace element composition and petrogenesis of natrocarbonatites. In: Bell K, Keller J (eds) Carbonatite volcanism: Oldoinyo Lengai and the petrogenesis of natrocarbonatites. Springer, Berlin Heidelberg New York, pp 70–86

Klemme S, van der Laan SR, Foley SF, Günther D (1995) Experimentally determined trace and minor element partitioning between clinopyroxene and carbonatite melt under upper mantle conditions. Earth Planet Sci Lett 133:439–448

Knudsen C (1991) Petrology, geochemistry and economic geology of the Qaquarssuk carbonatite complex, southern West Greenland. Monogr Ser on Mineral Deposits 29. Borntraeger, Berlin

Langmuir CH (1989) Geochemical consequences of in situ crystallization. Nature 340:199–205

Le Bas MJ (ed) (1977) Carbonatite–nephelinite volcanism: an African case history. Wiley, London

Le Bas MJ (1989) Diversification of carbonatite. In: Bell K (ed) Carbonatites: genesis and evolution. Unwin Hyman, London, pp 428–447

Le Bas MJ (1999) Sövite and alvikite: two chemically distinct calciocarbonatites C1 and C2. S Afr J Geol 102:109–121

Le Bas MJ, Handley C (1979) Variation in apatite composition in ijolitic and carbonatitic igneous rocks. Nature 279:54–56

Le Bas MJ, Keller J, Tao Kejie, Wall F, Williams CT, Zhang Peishan (1992) Carbonatite dykes at Bayan Obo, Inner Mongolia, China. Mineral Petrol 46:195–228

le Roex AP, Lanyon R (1998) Isotope and trace element geochemistry of Cretaceous Damaraland lamprophyres and

carbonatites, northwestern Namibia: evidence for plume–lithosphere interactions. J Petrol 39:1117–1146
Mariano AN (1989) Nature of economic mineralization in carbonatites and related rocks. In: Bell K (ed) Carbonatites: genesis and evolution. Unwin Hyman, London, pp 149–176
Minarik WG, Watson EB (1995) Interconnectivity of carbonate melt at low melt fraction. Earth Planet Sci Lett 133:423–437
Möller P, Dulski P (1999) LA-ICPMS study of REE and Y distribution in fluorite. In: Stanley CJ et al. (eds) Mineral deposits: processes to processing. Balkema, Rotterdam, pp 1133–1136
Möller P, Morteani G, Schley F (1980) Discussion of REE distribution patterns of carbonatites and alkalic rocks. Lithos 13:171–179
Morogan V, Lindblom S (1995) Volatiles associated with the alkaline–carbonatite magmatism at Alnö, Sweden: a study of fluid and solid inclusions in minerals from the Långarsholmen ring complex. Contrib Mineral Petrol 122:262–274
Nagasawa H (1970) Rare earth concentration in zircons and apatites and their host dacites and granites. Earth Planet Sci Lett 9:359–364
Nathan Y (1996) Mechanism of CO_3^{2-} substitution in carbonate–fluorapatite: evidence from FTIR spectroscopy, ^{13}C NMR, and quantum mechanical calculations – discussion. Am Mineral 81:513–514
Nelson DR, Chivas AR, Chappell BW, McCulloch MT (1988) Geochemical and isotopic systematics in carbonatites and implications for the evolution of ocean-island sources. Geochim Cosmochim Acta 52:1–17
Paster TP, Schauwecker DS, Haskin LA (1974) The behaviour of some trace elements during solidification of the Skaergaard layered intrusion. Geochim Cosmochim Acta 38:1549–1577
Prins P (1981) The geochemical evolution of the alkaline and carbonatite complexes of the Damaraland igneous province, South West Africa. Ann Univ Stellenbosch 3, Ser A1: 145–278
Rakovan J, Reeder RJ (1996) Intracrystalline rare earth element distributions in apatite: surface structural influences on incorporation during growth. Geochim Cosmochim Acta 60:4435–4445
Rankin AH (1975) Fluid inclusion studies in apatite from carbonatites of the Wasaki area of western Kenya. Lithos 8:123–136
Regnier P, Lasaga AC, Berner RA, Han OH, Zilm KW (1994) Mechanism of CO_3^{2-} substitution in carbonate–fluorapatite: evidence from FTIR spectroscopy, ^{13}C NMR, and quantum mechanical calculations. Am Mineral 79:809–818
Rimstidt JD, Balog A, Webb J (1998) Distribution of trace elements between carbonate minerals and aqueous solutions. Geochim Cosmochim Acta 62:1851–1863
Samson IM, Williams-Jones AE, Liu W (1995) The chemistry of hydrothermal fluids in carbonatites: evidence from leachate and SEM-decrepitate analysis of fluid inclusions from Oka, Quebec, Canada. Geochim Cosmochim Acta 59:1979–1989
Stoppa F, Liu L (1995) Chemical composition and genetic implications of apatites from some ultra-alkaline Italian rocks. Eur J Mineral 7:391–402
Stormer JC, Pierson ML, Tacker RC (1993) Variation of F and Cl X-ray intensity due to anisotropic diffusion in apatite during electron microprobe analysis. Am Mineral 78:641–648
Tepper JH, Kuehner SM (1999) Complex zoning in apatite from the Idaho batholith: a record of magma mixing and intracrystalline trace element diffusion. Am Mineral 84:581–595
Treiman AH, Schedl A (1983) Properties of carbonatite magma and processes in carbonatite magma chambers. J Geol 91:437–447
Vincze L (1995) Monte Carlo simulation of conventional and synchrotron XRF spectrometers. PhD Thesis, University of Antwerp
Walter AV, Flicoteaux R, Parron C, Loubet M, Nahon D (1995) Rare-earth elements and isotopes (Sr, Nd, O, C) in minerals from the Juquiá carbonatite (Brazil): tracers of a multistage evolution. Chem Geol 120:27–44
Watson EB, Green TH (1981) Apatite/liquid partition coefficients for the rare earth elements and strontium. Earth Planet Sci Lett 56:405–421
Wolff JA (1994) Physical properties of carbonatite magmas inferred from molten salt data, and application to extraction patterns from carbonatite–silicate magma chambers. Geol Mag 131:145–153
Wood SA (1990) The aqueous geochemistry of the rare-earth elements and yttrium 2. Theoretical predictions of speciation in hydrothermal solutions to 350 °C at saturation water vapor pressure. Chem Geol 88:99–125
Woolley AR, Kempe DRC (1989) Carbonatites: nomenclature, average chemical compositions, and element distribution. In: Bell K (ed) Carbonatites: genesis and evolution. Unwin Hyman, London, pp 1–14
Wyllie PJ (1989) Origin of carbonatites: evidence from phase equilibrium studies. In: Bell K (ed) Carbonatites: genesis and evolution. Unwin Hyman, London, pp 500–545
Zaitsev A, Bell K (1995) Sr and Nd isotope data of apatite, calcite and dolomite as indicators of source, and the relationships of phoscorites and carbonatites from the Kovdor massif, Kola peninsula, Russia. Contrib Mineral Petrol 121:324–335
Zhong S, Mucci A (1995) Partitioning of rare earth elements (REEs) between calcite and seawater solutions at 25 °C and 1 atm, and high dissolved REE concentrations. Geochim Cosmochim Acta 59:443–453